BI-TP 2008/04 Edinburgh 2008/07
FTUAM-08-01 FTUV-08-0226
IFIC/08-07 IFT-UAM-CSIC-08-07
MKPH-T-08-01

Determination of the $\Delta S = 1$ weak Hamiltonian in the SU(4) chiral limit through topological zero-mode wave functions

P. Hernández[a], M. Laine[b], C. Pena[c], E. Torró[a], J. Wennekers[d], H. Wittig[e]

[a] *Dpto. Física Teórica, Universidad de Valencia and IFIC-CSIC*
Apt. 22085, E-46071 Valencia, Spain

[b] *Faculty of Physics, University of Bielefeld, D-33501 Bielefeld, Germany*

[c] *Dpto. Física Teórica and Instituto de Física Teórica UAM/CSIC*
Facultad de Ciencias, Universidad Autónoma de Madrid
Cantoblanco, E-28049 Madrid, Spain

[d] *SUPA, School of Physics, University of Edinburgh, Edinburgh EH9 3JZ, UK*

[e] *Institut für Kernphysik, University of Mainz, D-55099 Mainz, Germany*

Abstract

A new method to determine the low-energy couplings of the $\Delta S = 1$ weak Hamiltonian is presented. It relies on a matching of the topological poles in $1/m^2$ of three-point correlators of two pseudoscalar densities and a four-fermion operator, measured in lattice QCD, to the same observables computed in the ϵ-regime of chiral perturbation theory. We test this method in a theory with a light charm quark, i.e. with an SU(4) flavour symmetry. Quenched numerical measurements are performed in a 2 fm box, and chiral perturbation theory predictions are worked out up to next-to-leading order. The matching of the two sides allows to determine the weak low-energy couplings in the SU(4) limit. We compare the results with a previous determination, based on three-point correlators containing two left-handed currents, and discuss the merits and drawbacks of the two procedures.

1. Introduction

Understanding quantitatively or even just qualitatively non-leptonic kaon decays, $K \to \pi\pi$, starting from the QCD Lagrangian, remains a formidable challenge despite decades of work. The difficulty is that the non-perturbative low-energy dynamics of strong interactions plays an essential role [1], yet it has turned out to be difficult to reduce the systematic errors of lattice studies of these effects [2, 3] to a tolerable level, because of the prohibitive cost of treating chiral symmetry, final state kinematics, and physical quark masses without compromises (for the current status and references, see ref. [4]).

A somewhat less challenging approach amounts to abandoning the direct computation of $K \to \pi\pi$ decay amplitudes in favour of determining, via lattice simulations, the low-energy couplings (LECs) of the effective chiral weak Hamiltonian that describes these decays [3]. This can be achieved by matching lattice measurements of suitable correlation functions to the same correlation functions computed within chiral perturbation theory (χPT). Among the simplifications thus achieved are that the matching does not necessitate physical kinematics, and that physical quark masses are not needed either, as long as the regime of validity of χPT is reached. This however requires sufficiently large volumes and small quark masses.

There are various possibilities for the order in which the volume is increased and the quark masses are decreased. In fact, it turns out to be useful to approach the chiral limit by first decreasing the quark masses. The reason is that in this parameter range, referred to as the ϵ-regime of χPT [5] (see also ref. [6]), it is possible to work out next-to-leading order corrections in χPT without introducing any more LECs than at the leading order, thereby putting the χPT side of the matching well under control.

At the same time, carrying out lattice simulations in the ϵ-regime is quite demanding. Fortunately, the advent of Ginsparg-Wilson formulations of lattice fermions [7]–[14], which possess an exact chiral symmetry in the limit of vanishing quark masses, and many subsequent developments on the numerical side [15], have made such simulations possible.

In ref. [16] a strategy based on these methods was proposed, with the goal of revealing the role that the charm quark mass plays in $K \to \pi\pi$ decays. The first step is the determination of the leading-order weak LECs in a theory with a light charm quark, that is in a four-flavour theory with an exact SU(4) chiral symmetry in the valence sector. The first results of this computation, from simulations in the ϵ-regime, have been presented in ref. [17]. The next step of the strategy is to increase the charm mass and monitor the LECs as we move towards a theory with an SU(3) flavour symmetry [16, 18].

The observables used for performing the matching between lattice QCD and the chiral effective theory in ref. [17] were three-point correlators of two left-handed currents and a weak operator. (The χPT side for these observables has also been worked out for SU(3) [19].) In this paper we pursue the same goal by means of a different type of observable. Indeed, we propose to consider a correlation function of two pseudoscalar densities and a weak operator. The peculiarity of this correlator is that it has poles in $1/m^2$ in the ϵ-regime, when evalu-

ated in sectors of non-vanishing topological charge (which we define à la ref. [20]). As we will show, the residues of these poles are easier to compute numerically than the correlation functions themselves, since they typically require fewer quark propagators, which are substituted by projectors on the zero-mode wave functions. We then use the residues to perform the matching between the fundamental and effective theories and determine the SU(4) weak LECs.

Let us stress that while the weak LECs themselves are universal, and can in principle be determined with any method, it is difficult to know *a priori* which of the multitude of possible strategies is the optimal one in practice. This depends, on one hand, on the numerical cost of the measurements involved, and on the other, on how well chiral perturbation theory converges for the observable in question. We will compare the two methods mentioned (ref. [17] and the present one) on both accounts. The hope is that by carrying out this comparison in the quenched approximation, it will become clear whether or not a particular strategy is superior when one moves to the more expensive unquenched environment, or if it remains the best policy to probe the LECs by a combination of independent techniques.

The paper is organized as follows. In Sec. 2 we introduce the observables to be computed in the fundamental theory and present the results of a next-to-leading order computation of the same observables in χPT, in the ϵ-regime. Besides the three-point functions previously mentioned, we will consider two-point functions that we use for normalization. In Sec. 3, we present the results of a quenched numerical computation of these amplitudes in a 2 fm box and a new determination of the weak LECs in the SU(4) limit. We conclude in Sec. 4.

2. Low-energy couplings from zero-mode wave functions

In the ϵ-regime and in a fixed topological sector, correlation functions involving quark propagators may contain poles in $1/(mV)^n$, where n is some integer, whenever the contribution of the zero-modes to the spectral representation of the quark propagator gives a non-vanishing contribution to the correlation function. For a number of reasons the residues turn out to be easier to compute than the correlation functions themselves. The idea, explored in detail in ref. [21], is then to use the residues of the topological poles to perform the matching between QCD and χPT, instead of the full correlation function. Given a correlation function $C_\nu(x_1, x_2, ...)$, the residue can be isolated by

$$C_\nu(x_1, x_2, ...) \equiv \frac{\mathrm{Res}_n}{(mV)^n} + ... \,, \qquad \mathrm{Res}_n = \lim_{m\to 0} (mV)^n C_\nu(x_1, x_2, ...) \,. \tag{2.1}$$

In ref. [21] the two-point function of the pseudoscalar density was considered in this context. The presence of a pole in $1/(mV)^2$ implies that the corresponding residue can be computed fully in terms of the zero-mode wave functions: no propagator computation is required. On the effective theory side, the same pole does appear and, up to a certain order, the residue is a function of only the pseudoscalar decay constant, F, and the volume (in the quenched theory

additional couplings appear). An exploratory numerical study in the quenched approximation was presented and the principal usefulness of the method to extract the low-energy coupling F was confirmed. Similar investigations have also been reported in refs. [22].

In the present work, we extend this idea to the computation of three-point functions from which the weak low-energy constants can be determined. In particular, we consider three-point functions of two pseudoscalar densities and a weak four-fermion operator. It is easy to see that such correlation functions do have poles in $1/(mV)^2$ when computed in non-trivial topological sectors in the ϵ-regime, as we now show.

2.1. Correlators in the fundamental theory

Following the strategy of refs. [16, 17], we consider a theory with four light and degenerate flavours such that $m_u = m_d = m_s = m_c = m$, which we refer to as the GIM limit. After integrating out the $W^\pm$ to first order in the weak coupling, $g_{\rm w}^2$, the resulting Weak Hamiltonian is given by

$$H_{\rm w} = \frac{g_{\rm w}^2}{4M_W^2} V_{us}^* V_{ud} \left\{ k_1^+ \; Z_{11}^+ Q_1^+ + k_1^- \; Z_{11}^- \; Q_1^- \right\} \; , \tag{2.2}$$

where the operators $Q_1^\pm$ transform in the **84** and **20** representations of SU(4):

$$Q_1^\pm = ([O_1]_{suud} \pm [O_1]_{sudu}) - (u \to c) \; , \tag{2.3}$$

$$[O_1]_{rsuv} \equiv (\bar\Psi_r \gamma_\mu P_- \tilde\Psi_u)(\bar\Psi_s \gamma_\mu P_- \tilde\Psi_v) \; . \tag{2.4}$$

Here $k_1^\pm$ are Wilson coefficients at the scale M_W, and $Z_{11}^\pm$ are the corresponding renormalization factors. We will follow the renormalization prescription of refs. [16, 17], that is we will use the RGI scheme, in which these factors are known non-perturbatively [23]. For any unexplained details we refer the reader to these references.

Deep in the non-perturbative regime this effective Hamiltonian admits an expansion in terms of the Goldstone boson fields and can be represented as

$$\mathcal{H}_{\rm w} = \frac{g_{\rm w}^2}{4M_W^2} V_{us}^* V_{ud} \left\{ g_1^+ \; \mathcal{Q}_1^+ + g_1^- \; \mathcal{Q}_1^- + ... \right\} \; , \tag{2.5}$$

where $\mathcal{Q}_1^\pm$ are operators made out of the Goldstone field, and terms of higher order in the chiral expansion have been omitted. Our task is to match for the coefficients $g_1^\pm$ in the chiral limit, by comparing lattice simulations with χPT predictions.

Now, given that QCD dynamics itself respects chiral symmetry, the results of such a matching are independent of the precise flavour indices appearing in eq. (2.3), as long as the operators remain traceless and have the correct symmetry properties. In practice, it is indeed convenient to consider the operators

$$O_1^\pm \equiv [O_1]_{rsuv} \pm [O_1]_{rsvu} \; , \tag{2.6}$$

with *all indices different*, rather than $Q_1^{\pm}$; these operators are automatically traceless, and no subtraction of the type in eq. (2.3) is needed. The results for the matching of $g_1^{\pm}$ are nevertheless guaranteed to be identical.

We want to carry out the matching in a finite volume through the computation of the following bare three-point functions in a fixed topological sector of charge ν:

$$A_\nu^{\pm}(x_0 - z_0, y_0 - z_0) \equiv - \lim_{m\to 0} (mV)^2 \int_{\mathbf{x}} \int_{\mathbf{y}} \langle \partial_{x_0} P^a(x) O_1^{\pm}(z) \partial_{y_0} P^b(y) \rangle_\nu \ , \tag{2.7}$$

where the bare pseudoscalar density reads $P^a \equiv i\bar{\Psi}\gamma_5 T^a \tilde{\Psi}$, and m is the bare quark mass. These amplitudes get contributions from two possible contractions, colour-disconnected, $\bar{A}_\nu$, and colour-connected, $\tilde{A}_\nu$:

$$A_\nu^{\pm} = (T^a_{ur} T^b_{vs} + T^a_{vs} T^b_{ur} \pm T^a_{vr} T^b_{us} \pm T^a_{us} T^b_{vr}) \Big[\bar{A}_\nu \pm \tilde{A}_\nu \Big] \ , \tag{2.8}$$

where

$$\begin{aligned}
\bar{A}_\nu &\equiv \lim_{m\to 0} (mV)^2 \int_{\mathbf{x}} \int_{\mathbf{y}} \partial_{x_0} \partial_{y_0} \mathrm{Tr}\left[S_m(x,z) \gamma_\mu P_- S_m(z,x) \gamma_5 \right] \mathrm{Tr}\left[S_m(y,z) \gamma_\mu P_- S_m(z,y) \gamma_5 \right] \ , \\
\tilde{A}_\nu &\equiv - \lim_{m\to 0} (mV)^2 \int_{\mathbf{x}} \int_{\mathbf{y}} \partial_{x_0} \partial_{y_0} \mathrm{Tr}\left[S_m(x,z) \gamma_\mu P_- S_m(z,y) \gamma_5 S_m(y,z) \gamma_\mu P_- S_m(z,x) \gamma_5 \right] \ .
\end{aligned} \tag{2.9}$$

Here S_m is the massive quark propagator.

It is convenient to normalize these three-point functions with bare two-point functions of the form

$$-i \mathrm{Tr}\left[T^a T^b\right] B_\nu(x_0 - z_0) \equiv \lim_{m\to 0} (mV) \int_{\mathbf{x}} \langle \partial_{x_0} P^a(x) L_0^b(z) \rangle_\nu \ , \tag{2.10}$$

where the bare left current reads $L_0^a \equiv \bar{\Psi}\gamma_0 P_- T^a \tilde{\Psi}$. Carrying out the contractions, we get

$$B_\nu(x_0 - z_0) = \lim_{m\to 0} (mV) \int_{\mathbf{x}} \partial_{x_0} \mathrm{Tr}\left[S_m(x,z) \gamma_0 P_- S_m(z,x) \gamma_5 \right] . \tag{2.11}$$

Note that the two-point function in eq. (2.10) can be related through the non-singlet axial Ward identity to the two-point function of two pseudoscalar densities, considered in ref. [21]:

$$\begin{aligned}
\mathrm{Tr}\left[T^a T^b\right] Z_A B_\nu(x_0 - z_0) &= i \lim_{m\to 0} (mV) \partial_{x_0} \int_{\mathbf{x}} \langle P^a(x) Z_A L_0^b(z) \rangle_\nu \\
&= -i \lim_{m\to 0} (mV) \partial_{z_0} \int_{\mathbf{z}} \langle P^a(x) Z_A L_0^b(z) \rangle_\nu \\
&= \lim_{m\to 0} (m^2 V) \int_{\mathbf{x}} \langle P^a(x) \ P^b(z) \rangle_\nu \ ,
\end{aligned} \tag{2.12}$$

where Z_A denotes the renormalization constant of the currents L_0^a. Here we made use of the fact that the product mP^a does not require renormalization.

Now, let us see why it is useful to consider the quantities in eqs. (2.9), (2.11). The point is that $\bar{A}_\nu, \tilde{A}_\nu$ and B_ν are zero, unless some of the quark propagators are saturated by zero modes. Let us denote by $v_i(x) \in \mathcal{K}$ the zero-mode wave functions (recall that the dimension of the kernel of the Dirac operator is $\dim(\mathcal{K}) = |\nu|$) that are normalized as

$$\int_x v_i^\dagger(x) v_i(x) = V \ . \tag{2.13}$$

The spectral representation of the quark propagator then reads

$$S_m(x,y) = \sum_{i=1}^{|\nu|} \frac{v_i(x) v_i^\dagger(y)}{mV} + \dots \ . \tag{2.14}$$

We can define the sources

$$\begin{aligned} \eta_i(z;x_0) &\equiv \partial_{x_0} \int_{\mathbf{x}} P_{-\chi} S_m(z,x) P_\chi v_i(x) \ , \\ \eta_i^\dagger(z;x_0) &= -\partial_{x_0} \int_{\mathbf{x}} v_i^\dagger(x) P_\chi S_m(x,z) P_{-\chi} \ , \end{aligned} \tag{2.15}$$

where χ is the chirality of the zero-modes. Given that $\gamma_\mu P_- = P_+ \gamma_\mu P_-$, we note that, depending on chirality, only some of the propagators can be saturated with zero-modes: for $\nu < 0$, the ones multiplying P_-, and for $\nu > 0$, the ones multiplying P_+. If $\nu > 0$, the disconnected and connected amplitudes of the three-point functions thus become

$$\begin{aligned} \bar{A}_\nu(x_0 - z_0, y_0 - z_0) &= \lim_{m\to 0} \ \frac{1}{L^3} \ \int_{\mathbf{z}} \Big\langle \sum_{i=1}^{|\nu|} v_i^\dagger(z) \gamma_\mu \eta_i(z;x_0) \sum_{j=1}^{|\nu|} v_j^\dagger(z) \gamma_\mu \eta_j(z;y_0) \Big\rangle_\nu \ , \\ \tilde{A}_\nu(x_0 - z_0, y_0 - z_0) &= -\lim_{m\to 0} \ \frac{1}{L^3} \ \int_{\mathbf{z}} \Big\langle \sum_{i,j=1}^{|\nu|} v_i^\dagger(z) \gamma_\mu \eta_j(z;y_0) v_j^\dagger(z) \gamma_\mu \eta_i(z;x_0) \Big\rangle_\nu \ , \end{aligned} \tag{2.16}$$

while for $\nu < 0$ we get

$$\begin{aligned} \bar{A}_\nu(x_0 - z_0, y_0 - z_0) &= \lim_{m\to 0} \ \frac{1}{L^3} \ \int_{\mathbf{z}} \Big\langle \sum_{i=1}^{|\nu|} \eta_i^\dagger(z;x_0) \gamma_\mu v_i(z) \sum_{j=1}^{|\nu|} \eta_j^\dagger(z;y_0) \gamma_\mu v_j(z) \Big\rangle_\nu \ , \\ \tilde{A}_\nu(x_0 - z_0, y_0 - z_0) &= -\lim_{m\to 0} \ \frac{1}{L^3} \ \int_{\mathbf{z}} \Big\langle \sum_{i,j=1}^{|\nu|} \eta_i^\dagger(z;x_0) \gamma_\mu v_j(z) \eta_j^\dagger(z;y_0) \gamma_\mu v_i(z) \Big\rangle_\nu \ . \end{aligned} \tag{2.17}$$

For the two-point function of eq. (2.11), the positive chirality case $\nu > 0$ yields

$$B_\nu(x_0 - z_0) = \lim_{m\to 0} \ \frac{1}{L^3} \int_{\mathbf{z}} \Big\langle \sum_{i=1}^{|\nu|} v_i^\dagger(z) \gamma_0 \eta_i(z;x_0) \Big\rangle_\nu \ , \tag{2.18}$$

while for $\nu < 0$ we arrive at

$$B_\nu(x_0 - z_0) = \lim_{m\to 0} \frac{1}{L^3} \int_{\mathbf{z}} \Big\langle \sum_{i=1}^{|\nu|} \eta_i^\dagger(z; x_0)\gamma_0 v_i(z) \Big\rangle_\nu \,. \tag{2.19}$$

Finally, the Ward identity of eq. (2.12) implies

$$Z_A B_\nu(x_0 - z_0) = D_\nu(x_0 - z_0) \equiv \frac{1}{V} \sum_{i,j=1}^{|\nu|} \int_{\mathbf{x}} \Big\langle v_j^\dagger(x) v_i(x) v_i^\dagger(z) v_j(z) \Big\rangle_\nu \,. \tag{2.20}$$

Here the limit $m \to 0$ has been taken analytically on the right-hand side, while it needs to be taken numerically on the left-hand side (cf. eqs. (2.18), (2.19)); therefore eq. (2.20) provides a non-trivial test on our ability to approach the limit needed in eqs. (2.16)–(2.19).

It is clear from eqs. (2.16)–(2.19) that a number of inversions equal to twice the topological charge, i.e. $2|\nu|$ (since x_0 and y_0 need to be fixed), is sufficient for constructing the correlation functions, whilst averaging over all the spatial positions of the three sources. When employing the method of refs. [16, 17], which is based on the left-handed current, the summation over the spatial positions of the three sources is only possible through low-mode averaging (LMA) [24, 25], and only for the contributions of the low modes. The price of LMA is $12 + 2 \times N_{\rm low}$ inversions, where $N_{\rm low}$ was the number of low modes treated separately. Typically $N_{\rm low}$ can be as large as 20 for 2 fm boxes, and hence the numerical cost can be quite substantial.

On the other hand, if the low modes of the Dirac operator are known, as for example would be the case if low-mode preconditioning [15] is used, it is possible to perform an additional averaging over time translations for the low-mode contributions to the correlation functions defined above. It is important to stress however that this extra low-mode averaging does not involve any additional inversion, therefore *the overhead is not proportional to* N_{low}, as in the standard case [24]. We will describe briefly how this works in section 3.1.

Summarizing, in order to perform the matching between the fundamental weak Hamiltonian and the effective one, we will be considering the bare ratios

$$R_\nu^\pm \equiv \frac{\bar{A}_\nu(x_0 - z_0, y_0 - z_0) \pm \tilde{A}_\nu(x_0 - z_0, y_0 - z_0)}{B_\nu(x_0 - z_0) B_\nu(y_0 - z_0)} \,. \tag{2.21}$$

The renormalized ratios needed for matching the LECs in eq. (2.5) are then obtained by multiplying these correlators by the renormalization factors $Z_{11}^\pm / Z_A^2$ (cf. eq. (2.41) below); the procedure is identical to the one in ref. [17] and we refer to that reference for details.

2.2. Correlators in chiral perturbation theory

We now present the results for the observables just defined in the Chiral Effective Theory.

2.2.1. Two-point function

The two-point correlation function that needs to be computed in χPT, corresponding to eq. (2.10), is given by

$$-i\mathrm{Tr}\,[T^aT^b]\mathcal{B}_\nu(x_0-z_0) \equiv \lim_{m\to 0}(mV)\partial_{x_0}\int_{\mathbf{x}}\langle \mathcal{P}^a(x)\ \mathcal{J}_0^b(z)\rangle_\nu\ , \tag{2.22}$$

where

$$\mathcal{J}_\mu^a = \frac{F^2}{2}\mathrm{Tr}\left[T^aU\partial_\mu U^\dagger\right] + ...\ , \tag{2.23}$$

$$\mathcal{P}^a = i\frac{\Sigma}{2}\mathrm{Tr}\left[T^a(U-U^\dagger)\right] + ...\ , \tag{2.24}$$

and contact terms have been omitted from eq. (2.22).

Since the mass is taken to zero in eq. (2.22), the computation is carried out according to the rules of the ϵ-expansion [5]. We work up to next-to-leading order (NLO). The results for the contributions of the individual graphs, as well as the various zero-mode and spacetime integrals appearing, are listed in appendix A.

Defining $\tau_x \equiv (x_0-z_0)/T$ and $\rho \equiv T/L$, and considering the unquenched theory, the final result from eq. (A.29) becomes, after replacing $E(x) = G(x)/N_\mathrm{f}$ and using eq. (A.27),

$$T\mathcal{B}_\nu(x_0-z_0) = |\nu|\left\{1+\frac{2\rho}{(FL)^2}\Big(|\nu|+\frac{1}{N_\mathrm{f}}\Big)h_1(\tau_x)\right\}\ , \tag{2.25}$$

where

$$h_1(\tau) \equiv \frac{1}{2}\left\{\left[(\tau \bmod 1)-\frac{1}{2}\right]^2-\frac{1}{12}\right\}\ . \tag{2.26}$$

In Fig. 1 we show this result for different values of $|\nu|$ in a symmetric box of size $T=L=2$ fm. The LO results are constants at $|\nu|$, so that all time dependence results from the subleading corrections.

In the quenched case we consider the ϵ-counting described in ref. [21], introduced in order to set up a parametrically convergent perturbative series. As explained there, three new couplings can in principle appear at NLO: α, m_0^2, K. The effect of α is to replace $1/N_\mathrm{f} \to \alpha/2N_\mathrm{c}$; however, this contribution is suppressed in the counting of ref. [21] and will be omitted. Similarly, contributions from m_0^2 are also suppressed and omitted. On the other hand, effects from the coupling K could be of order unity, and need to be studied explicitly.

The coefficient K has two main effects. First of all, the pseudoscalar density is modified to

$$P^a = i\frac{\Sigma}{2}\mathrm{Tr}\left[T^a(U-U^\dagger)\right] - K\Phi_0\mathrm{Tr}\left[T^a(U+U^\dagger)\right] + ...\ , \tag{2.27}$$

where we have for brevity kept the notation of the unquenched theory, usable in the replica formulation of quenched χPT [26]; for the notation in the supersymmetric formulation [27],

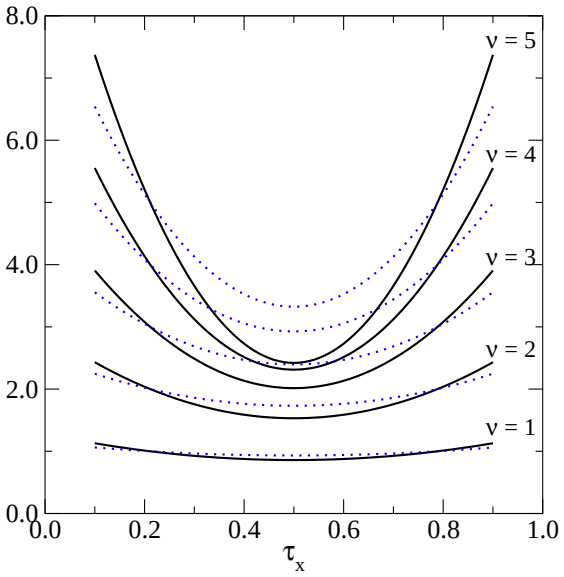

Figure 1: The two-point correlation function $T\mathcal{B}_\nu(x_0 - z_0)$ for $N_{\rm f} = 2$ (solid) and $N_{\rm f} = 0$ (dotted) as a function of $\tau_x = (x_0 - z_0)/T$, for $T = L = 2$ fm. The pion decay constant F has been fixed to 93 MeV for $N_{\rm f} = 2$ and to 110 MeV for $N_{\rm f} = 0$.

see eq. (3.2) of ref. [21]. In eq. (2.27), $\Phi_0 = \frac{F}{2}\mathrm{Tr}\,[-i \ln U]$ is the singlet field. Second, the zero-mode integration measure is modified:

$$\langle ... \rangle_\nu^q = \frac{\int_{U_0 \in U(N)} (...)\, \det{}^\nu U_0 \, \exp\left[\frac{\mu}{2}\mathrm{Tr}\,(U_0 + U_0^\dagger) + 2\nu\frac{mKN_{\rm c}}{m_0^2 F}\mathrm{Tr}\,(U_0 - U_0^\dagger)\right]}{\int_{U_0 \in U(N)} \det{}^\nu U_0 \, \exp\left[\frac{\mu}{2}\mathrm{Tr}\,(U_0 + U_0^\dagger) + 2\nu\frac{mKN_{\rm c}}{m_0^2 F}\mathrm{Tr}\,(U_0 - U_0^\dagger)\right]} \,. \qquad (2.28)$$

To first order in K, the effects come from the standard tree-level contribution computed with the modified weight of eq. (2.28), and from a new tree-level term containing the K-term from eq. (2.27).

The results for the two new contributions are given in eqs. (A.14), (A.15) of appendix A. However, inserting the zero-mode integrals from eqs. (A.24), (A.25), these contributions cancel against each other. Therefore,

$$T\mathcal{B}_\nu^q(x_0 - z_0) \;\; = \;\; |\nu|\left\{1 + \frac{2\rho|\nu|}{(FL)^2} h_1(\tau_x)\right\}, \qquad (2.29)$$

and the result is very close to that in the full theory (were it not that F is different). Some examples are shown in Fig. 1.

2.2.2. Three-point function

Next we consider the three-point function corresponding to eq. (2.7) in χPT :

$$\mathcal{A}_\nu^\pm(x_0-z_0,y_0-z_0) \equiv -\lim_{m\to 0}(mV)^2\int_{\mathbf{x}}\int_{\mathbf{y}}\langle \partial_{x_0}\mathcal{P}^a(x)\mathcal{O}_1^\pm(z)\partial_{y_0}\mathcal{P}^b(y)\rangle_\nu \,. \tag{2.30}$$

Here, like in eq. (2.6),

$$\mathcal{O}_1^\pm \equiv [\mathcal{O}_1]_{rsuv} \pm [\mathcal{O}_1]_{rsvu} \,, \tag{2.31}$$

where the weak operators are given by

$$\mathcal{O}_{rsuv} = \frac{F^4}{4}\,\Big(\partial_\mu UU^\dagger\Big)_{ur}\Big(\partial_\mu UU^\dagger\Big)_{vs} + \ldots \,. \tag{2.32}$$

Again, contact terms have been omitted from eq. (2.30).

Like for the two-point function, we work up to NLO. The results for the contributions of the individual graphs, as well as the various zero-mode and spacetime integrals appearing, are listed in appendix B.

The result obtained after summing together all the graphs can be written as

$$\mathcal{A}_\nu^\pm = (T^a_{ur}T^b_{vs} + T^a_{vs}T^b_{ur} \pm T^a_{vr}T^b_{us} \pm T^a_{us}T^b_{vr})\Big[\bar{\mathcal{A}}_\nu \pm \tilde{\mathcal{A}}_\nu\Big] \,, \tag{2.33}$$

where, inserting $E(x) = G(x)/N_{\rm f}$ into eq. (B.33) and using eq. (B.28), one obtains

$$\begin{aligned}\bar{\mathcal{A}}_\nu \pm \tilde{\mathcal{A}}_\nu = \Big(1 \mp \frac{1}{|\nu|}\Big)\Big\{&\mathcal{B}_\nu(x_0-z_0)\mathcal{B}_\nu(y_0-z_0)\\ \pm\ &\frac{\nu^2}{F^2V}\Big[2\beta_1\rho^{-\frac{3}{2}} + f_1(\tau_x) + f_1(\tau_y) - h_1(\tau_x) - h_1(\tau_y) + \Big(1\mp\frac{2}{N_{\rm f}}\Big)H(\tau_x,\tau_y)\Big]\Big\} \,.\end{aligned} \tag{2.34}$$

Here $\tau_x \equiv (x_0-z_0)/T$, $\tau_y \equiv (y_0-z_0)/T$, $\rho \equiv T/L$, β_1 is a *shape coefficient* depending on the value of ρ [28, 29], the function h_1 is defined in eq. (2.26), and

$$H(\tau_x,\tau_y) \equiv h_1'(\tau_x)h_1'(\tau_y) - h_1(\tau_x-\tau_y) - \Big[h_1'(\tau_x) - h_1'(\tau_y)\Big]h_1'(\tau_x-\tau_y) \,, \tag{2.35}$$

$$f_1(\tau) \equiv \big[h_1'(\tau)\big]^2 + \sum_{\mathbf{p}\neq 0}\big[|\mathbf{p}|^2 C_{\mathbf{p}}(\tau)^2 + C'_{\mathbf{p}}(\tau)^2\big] \,. \tag{2.36}$$

Furthermore, $\mathbf{p} = 2\pi\rho\,\mathbf{n}$ with $\mathbf{n} = (n_1,n_2,n_3)$ being a vector of integers, and

$$C_{\mathbf{p}}(\tau) \equiv \frac{\cosh\big\{|\mathbf{p}|\,\big[(\tau \bmod 1) - \frac{1}{2}\big]\big\}}{2|\mathbf{p}|\sinh(|\mathbf{p}|/2)} \,, \quad C'_{\mathbf{p}}(\tau) = \frac{\sinh\big\{|\mathbf{p}|\,\big[(\tau \bmod 1) - \frac{1}{2}\big]\big\}}{2\sinh(|\mathbf{p}|/2)} \,. \tag{2.37}$$

The first term in eq. (2.34) has the form of a factorized contribution. We can cancel out this term by taking the ratio of the three-point function with respect to the product of two two-point functions, in analogy with eq. (2.21):

$$\mathcal{R}_\nu^\pm \equiv \frac{\bar{\mathcal{A}}_\nu(x_0-z_0,y_0-z_0) \pm \tilde{\mathcal{A}}_\nu(x_0-z_0,y_0-z_0)}{\mathcal{B}_\nu(x_0-z_0)\mathcal{B}_\nu(y_0-z_0)} \tag{2.38}$$

$$\equiv \Big(1\mp\frac{1}{|\nu|}\Big)\Big[1 \pm r_\pm(z_0)\Big] \,. \tag{2.39}$$

We have adopted a notation here where x_0, y_0 are assumed fixed, so that $r_\pm$ is a function of z_0 only. Inserting the tree-level result $\mathcal{B}_\nu = |\nu|/T$ in the numerators when dividing the NLO correction, we then obtain from eq. (2.34) that

$$r_\pm(z_0) = \frac{\rho}{(FL)^2}\Big[2\beta_1\rho^{-\frac{3}{2}} + f_1(\tau_x) + f_1(\tau_y) - h_1(\tau_x) - h_1(\tau_y) + \Big(1 \mp \frac{2}{N_{\rm f}}\Big)H(\tau_x,\tau_y)\Big] \ . \quad (2.40)$$

Note that $r_\pm$ is independent of ν, i.e. the topology and volume dependences have completely factorized at this order. The low-energy couplings $g_1^\pm$ can now be obtained from the matching

$$g_1^\pm \mathcal{R}_\nu^\pm = k_1^\pm \ \frac{Z_{11}^\pm}{Z_A^2} \ R_\nu^\pm \ , \quad (2.41)$$

at sufficiently large distances between the sources.

The quenched result in the counting of ref. [21] is obtained by simply leaving out the term $1/N_{\rm f}$, because terms involving α and m_0^2 are of higher order, like for the two-point correlator, and effects from the coupling K cancel at this order, as demonstrated in appendix B (cf. eqs. (B.13), (B.14), (B.20), (B.21)):

$$r_\pm^q(z_0) = \frac{\rho}{(FL)^2}\Big[2\beta_1\rho^{-\frac{3}{2}} + f_1(\tau_x) + f_1(\tau_y) - h_1(\tau_x) - h_1(\tau_y) + H(\tau_x,\tau_y)\Big] \ . \quad (2.42)$$

The most efficient way of evaluating numerically the amplitudes $\bar{A}_\nu$ and $\tilde{A}_\nu$ is by fixing the temporal position of the sources, x_0 and y_0, so that the three-point correlator is measured as a function of the temporal position of the weak operator, z_0. In order to maximize the separation between the three operators we take $x_0 \sim T/3$ and $y_0 \sim T - x_0$. The signal should be best when the weak operator is near the origin, and simultaneously the NLO correction $r_\pm(z_0)$ is minimized. The corresponding values of $(FL)^2 r_\pm^q(0)$ for various box shapes are given in Table 1. There is a very strong dependence on z_0 (cf. Fig. 2) which results from the fact that the functions $f_1(\tau_x)$ and $f_1(\tau_y)$ are divergent at $\tau_x = 0$ and $\tau_y = 0$, respectively, while they fall off exponentially, $\sim \exp(-2\pi\rho\tau_x)$, $\sim \exp(-2\pi\rho\tau_y)$, away from these points[1]. Thereby a way to decrease these corrections is to increase $\rho = T/L$ [2]. In this respect the situation is opposite to that in ref. [17] where left-handed currents appear in place of pseudoscalar densities; then the NLO corrections increase rapidly with $T/L \gtrsim 2$ [16].

Fig. 2 shows the result for $1 \pm r_\pm^q$ for various box volumes, for $x_0 = T/3$, $y_0 = 2T/3$. Unfortunately, NLO corrections seem to be rather large at $L = 2$ fm.

[1] These terms could be decreased by increasing τ_x, τ_y towards 1/2, since nothing dramatic happens as $\tau_x \to \tau_y$ according to NLO expressions (cf. Table 1). However, this situation may be specific to the SU(4) case, where there are no quark propagators connecting the pseudoscalar densities, while in the physical SU(3) case it is probably reasonable to keep the pseudoscalar densities somewhat apart from other.

[2] Note however that increasing ρ takes us closer to the so-called δ-regime [30].

V	x_0/a	y_0/a	τ_x	τ_y	$(FL)^2 r_\pm^q(0)$
16^4	4	12	0.25000	0.75000	0.89309
16^4	5	11	0.31250	0.68750	0.62839
16^4	6	10	0.37500	0.62500	0.51281
16^4	7	9	0.43750	0.56250	0.41875
$16^3 32$	11	21	0.34375	0.65625	0.45251
$16^3 32$	12	20	0.37500	0.62500	0.43174
$16^3 32$	13	19	0.40625	0.59375	0.38822
$16^3 32$	14	18	0.43750	0.56250	0.32157
$16^3 32$	15	17	0.46875	0.53125	0.23162
24^4	8	16	0.33333	0.66667	0.58270
24^4	9	15	0.37500	0.62500	0.51281
24^4	10	14	0.41667	0.58333	0.45099
24^4	11	13	0.45833	0.54167	0.38435

Table 1: Examples of values of $(FL)^2 r_\pm^q(0)$ for various box shapes. Note that in the quenched limit, $r_\pm^q(0)$ is independent of the channel $\pm$, cf. eq. (2.42).

	β	r_0/a	V	$N_{\rm low}$	$\lvert\nu\rvert$	$N_{\rm conf}^{\lvert\nu\rvert}$	$\frac{x_0}{a}$, $\frac{y_0}{a}$	Z_A	am
A_1	5.8458	4.026	16^4	20	1-5	118,94 99,73,65	5,11	1.710	0.0015,0.0025, 0.005
A_2	6.0735	6.072	24^4	20	2-5	92,63 51,55	8,16	1.505	0.002, 0.0033, 0.0067

Table 2: Parameters of the simulations.

3. Numerical results

We have carried out a numerical test of the method outlined above, in the quenched approximation. Table 2 shows the simulation parameters. We have considered a symmetric lattice $T = L \simeq 2$ fm at two different lattice spacings in order to test for scaling violations in these observables.

To evaluate the correlation functions of eqs. (2.16)–(2.19), we have computed chiral quark propagators on quenched background gauge configurations, using the Neuberger-Dirac operator with $s = 0.4$. For all details of the numerical implementation we refer the reader to refs. [15, 24, 16], whose techniques we adopt.

Before presenting the actual data, let us describe how low-mode averaging (LMA) can be

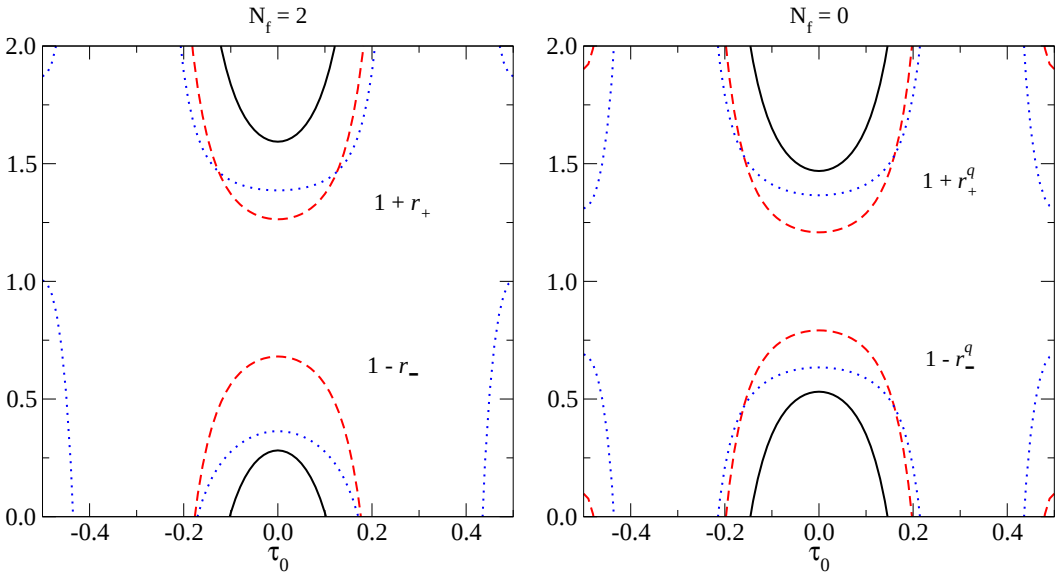

Figure 2: The functions $1 \pm r_\pm$ (eq. (2.39)) for $N_\mathrm{f} = 2$ (left) and $N_\mathrm{f} = 0$ (right) as a function of $\tau_0 \equiv z_0/T$, for $x_0 = T/3$, $y_0 = 2T/3$. The pion decay constant F has been fixed to 93 MeV for $N_\mathrm{f} = 2$ and to 110 MeV for $N_\mathrm{f} = 0$. The solid line corresponds to $T = L$ =2 fm, the dashed to $T = L = 3$ fm, and the dotted to $T/2 = L$ =2 fm.

used to reduce statistical fluctuations in the signal.

3.1. Low-mode averaging

Our observables, eqs. (2.16)–(2.19), involve both zero-mode wave functions and actual quark propagators. Since we employ low-mode preconditioning [15] for determining the quark propagators, which requires the computation of a few lowest eigenvectors of the Dirac operator, we can use these in order to perform an extra averaging over time translations of the low-mode contribution to eqs. (2.16)–(2.19). In other words, the LMA technique [24, 25] gives only an extra averaging over time in our case, but is nevertheless helpful as we will see, since the numerical overhead involved is negligible.

The main idea of LMA is to substitute the chiral propagator in eqs. (2.16)–(2.19) by

$$P_{-\chi} S_m(z,x) P_\chi = \sum_{k=1}^{N_\mathrm{low}} \Psi_k(z) \otimes \Psi_k^\dagger(x) + P_{-\chi} S_m^\mathrm{sub}(z,x) P_\chi \;, \tag{3.1}$$

where $S_m^\mathrm{sub}(z,x)$ is the inverse of the massive Dirac operator in the subspace orthogonal to the eigenspace of the approximate low-modes, and the chiral components of Ψ_k are given by

$$P_{-\chi}\Psi_k(x) = w_k(x), \quad P_\chi \Psi_k(x) = \frac{1}{\alpha_k} P_\chi \gamma_5 D P_{-\chi} w_k(x) \;, \tag{3.2}$$

where $w_k(x)$ are the approximate eigenfunctions of the operator $D^\dagger D$ for the eigenvalue λ_k, while $\alpha_k = \sqrt{\lambda_k}$. We indicate how this works with the two-point correlator.

The LMA evaluation of eq. (2.18) is based on the separation

$$B_\nu \;=\; B_\nu^l + B_\nu^h, \tag{3.3}$$

where the "high-mode part" reads

$$B_\nu^h(x_0 - z_0) \;=\; \lim_{m\to 0}\; \frac{1}{L^3}\int_{\mathbf{z}} \Big\langle \sum_{i=1}^{|\nu|} v_i^\dagger(z)\gamma_0 \tilde{\eta}_i(z;x_0)\Big\rangle_\nu , \tag{3.4}$$

with

$$\tilde{\eta}_i(z;x_0) \equiv \partial_{x_0}\int_{\mathbf{x}} P_{-\chi} S_m^{\rm sub}(z,x) P_\chi v_i(x)\ , \tag{3.5}$$

while the low-mode contribution is

$$B_\nu^l(t) \;=\; \lim_{m\to 0}\; \sum_{i=1}^{|\nu|}\sum_{k=1}^{N_{\rm low}} \frac{1}{V}\int_{x,z} \delta(x_0 - z_0 - t)\left\langle v_i^\dagger(z)\gamma_0 P_- \Psi_k(z)\partial_{x_0}\left[\Psi_k^\dagger(x) P_+ v_i(x)\right]\right\rangle_\nu\ . \tag{3.6}$$

The LMA evaluation of the three-point function is carried out in complete analogy.

3.2. Two-point function

In Fig. 3 we show results for the two-point correlator $B_\nu(t)$ (cf. eqs. (2.18), (2.19)) in different topological sectors at the lightest quark mass. The open/full symbols corresponds to the results without/with LMA. There is a strong dependence on $|\nu|$, as expected from χPT.

Since there is clear evidence for NLO corrections, we consider a two-parameter fit of the form

$$TB_\nu(t) = \alpha_\nu + 2\beta_\nu h_1(\tau)\ , \quad \tau = \frac{t}{T}\ , \tag{3.7}$$

where h_1 is from eq. (2.26). The temporal dependence in all sectors is perfectly compatible with the function $h_1(\tau)$ as illustrated by the solid lines in Fig. 3, which are the results of the fits in the time interval $\Delta t = 5a - 11a$. The small dependence on the quark mass is perfectly linear, so the values of α_ν and β_ν are linearly extrapolated to the zero mass limit. The results for α_ν and β_ν in the chiral limit are summarized in Table 3. The jackknife procedure has been used to estimate the errors.

In Fig. 4 we show the results for α_ν and β_ν as a function of $|\nu|$, together with the NLO expectations. In the case of α_ν, the NLO prediction $\alpha_\nu = |\nu|$ is extremely well reproduced at the per cent level. The prediction for β_ν, on the other hand, depends on F. The dashed line in the figure corresponds to a fit to the NLO prediction leaving F as a free parameter. The best fit values are $(FL)_{\rm A_1} = 1.19(2)$ and $(FL)_{\rm A_2} = 1.14(2)$ with $\chi^2/{\rm d.o.f} \sim 9$ and 12, respectively,

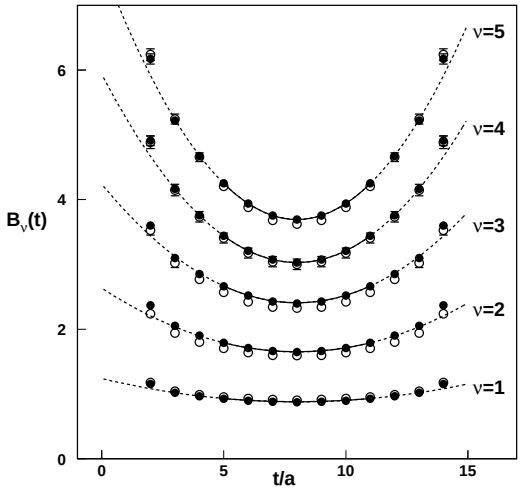

Figure 3: The measured $TB_\nu(t)$ for lattice A_1 and quark mass $am = 0.0015$. Open/full symbols correspond to data without/with LMA. Error bars are in most cases smaller than the symbol sizes.

which are rather bad. Clearly the $|\nu|$ dependence is not properly reproduced at NLO, however it seems that the discrepancy could be ascribed to higher order chiral corrections.

We have seen that the Ward identity, eq. (2.12), relates $B_\nu(t)$ to the topological zero-mode contribution in the correlator of two pseudoscalar densities. This quantity was studied in ref. [21], and actually the chiral corrections were computed to one order higher than here. Although the expressions are rather complicated and involve new time-dependent functions, a convenient way to try to include these corrections is to consider a Taylor expansion around the middle point, $t = T/2$. From the results of ref. [21], we expect that

$$TB_\nu(t) = \gamma_\nu + \delta_\nu \left(\frac{t}{T} - \frac{1}{2}\right)^2 + \ldots \,, \tag{3.8}$$

where[3]

$$\delta_\nu = \frac{\rho}{(FL)^2} \left\{ \nu^2 + \frac{\rho|\nu|}{(FL)^2} \left[-\beta_1 \rho^{-\frac{3}{2}} - \frac{1}{24}\left(\frac{7}{3} + 2\nu^2 - 2\langle\nu^2\rangle\right) + \frac{\gamma_1}{2} \right] \right\} . \tag{3.9}$$

For a symmetric box with $T = L$ the shape coefficients read $\rho = 1$, $\beta_1 = 0.14046098$, and $\gamma_1 = -0.05712765$.

Numerically the results for δ_ν in a fit of the form in eq. (3.8) are identical to those for β_ν in Table 3. The solid line in the lower plot of Fig. 4 corresponds to the prediction of eq. (3.9)

[3]We have set $\alpha = 0$, since this parameter was consistent with zero in the analysis of ref. [21].

$\|\nu\|$	$\alpha_\nu(\mathrm{A}_1)$	β_ν (A_1)	$\alpha_\nu(\mathrm{A}_2)$	β_ν (A_2)
1	1.00(1)	1.4(3)		
2	1.98(2)	3.9(4)	2.02(2)	4.5(4)
3	3.02(3)	7.3(4)	3.00(3)	8.8(5)
4	4.00(4)	11.6(5)	3.97(4)	11.9(5)
5	5.01(5)	15.8(6)	5.00(4)	17.7(6)

Table 3: Results for α_ν and β_ν from a fit to eq. (3.7) of the measured two-point correlator, subsequently extrapolated to the zero-mass limit.

using $\langle \nu^2 \rangle = \chi_t V = 0.059 V/r_0^4$ [31] and leaving F as a free parameter. The result of the fit is $(FL)_{\mathrm{A}_1} = 1.12(2)$ and $(FL)_{\mathrm{A}_2} = 1.07(2)$ with $\chi^2/\mathrm{d.o.f} = 0.2, 1.3$, respectively. The results for F are essentially the same as the central values in ref. [21] (this is almost trivial in the light of Sec. 3.3 below)[4]; however, the current error bars are much smaller, because higher topological sectors which are less noisy have been considered. Besides, we have not assigned any errors to α and χ_t, as we did in [21]. The results are in reasonable agreement also with the determination of F from the left-current two-point correlator in ref. [24], although it must be noted that the box size was significantly smaller there.

3.3. Ward identity and chiral extrapolation

The Ward identity of eq. (2.12) is a good test of the extrapolation $m \to 0$ needed for the correlator $B_\nu(t)$.

In Fig. 5 we show results for the ratio $Z_A \equiv D_\nu(t)/B_\nu(t)$ (notation as in eq. (2.20)) as a function of am for the different topological sectors, normalized to the value $\hat{Z}_A$ obtained by conventional means in ref. [32]. In the limit $m \to 0$, the ratio should approach unity in all topological sectors. The level of agreement between the different sectors and with $\hat{Z}_A$ is shown in Table 4. Given that only the zero-mode contributions to both sides of the Ward Identity are included, this is a strong check of the whole procedure, and furthermore indicates that the small residual extrapolation to zero quark mass is under good control.

3.4. Three-point function

In Fig. 6 we show one example of a Monte Carlo history for the three-point functions $\bar{A}_\nu \pm \tilde{A}_\nu$, eqs. (2.16), (2.17), with and without LMA. Clearly LMA improves the signal significantly.

[4]Note that a similar physical box size was used in ref. [21] as in the present study.

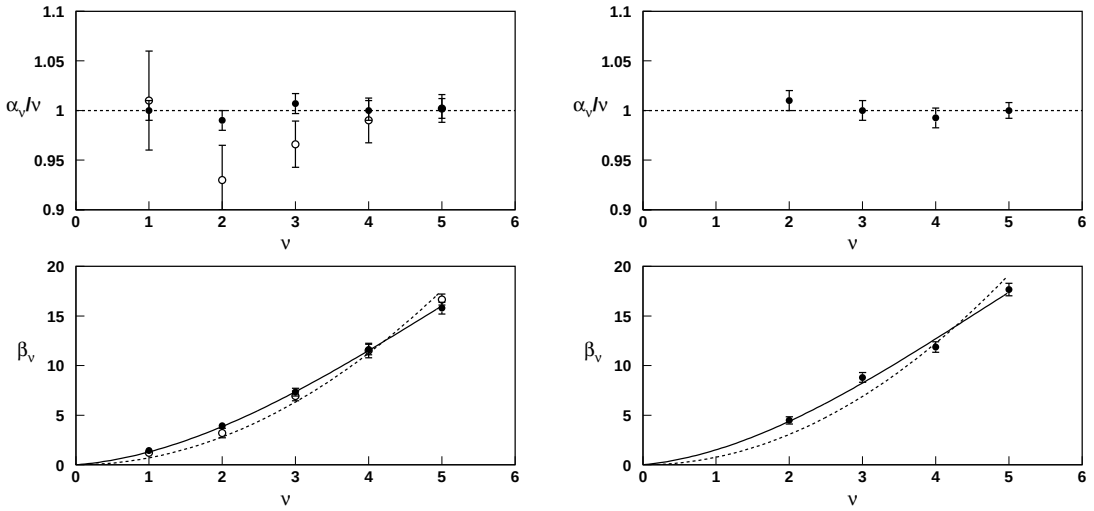

Figure 4: Top: $\alpha_\nu/|\nu|$ versus $|\nu|$ for lattice A_1 (left) and lattice A_2 (right). The dashed line is the NLO expectation. Bottom: β_ν versus $|\nu|$ for the same lattices. The dashed line is the best fit NLO prediction, the solid line is the best fit NNLO prediction. In both cases open/full symbols correspond to without/with LMA.

$\lvert\nu\rvert$	$Z_A/\hat{Z}_A(\mathrm{A}_1)$	$Z_A/\hat{Z}_A(\mathrm{A}_2)$
1	1.000(6)	
2	1.009(4)	0.991(3)
3	0.999(4)	0.995(3)
4	1.008(3)	0.999(3)
5	1.000(3)	1.002(3)

Table 4: The ratio $Z_A \equiv D_\nu/B_\nu$ (cf. eq. (2.20)), obtained from the saturation with zero modes of the Ward Identity (with LMA treatment of the non-zero mode part of B_ν), normalized to the conventionally determined $\hat{Z}_A$ [32]. The errors do not include the error on $\hat{Z}_A$ which is about 3 per mille.

The improvement is more pronounced for the smaller topologies and masses as expected. In all of the following we consider only the LMA results.

In Figs. 7, 8 we show the results for the bare ratios $R_\nu^{\pm}(x_0-z_0, y_0-z_0)/(1\mp 1/|\nu|)$ on lattice

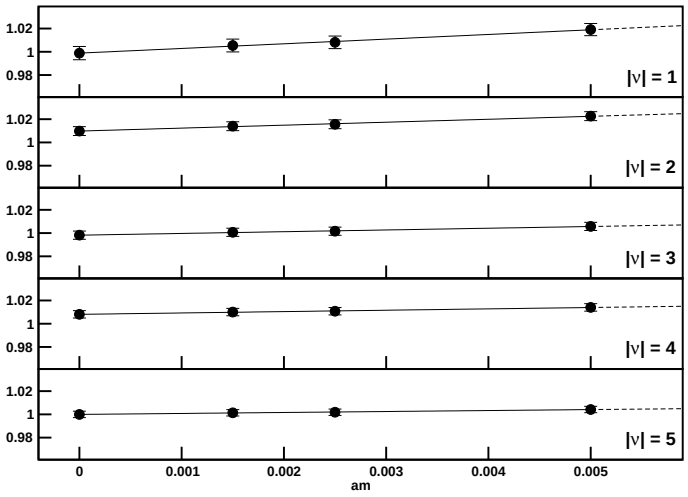

Figure 5: Chiral extrapolation of the time-averaged ratio $D_\nu(t)/B_\nu(t)$ (cf. eq. (2.20)) normalized to $\hat{Z}_A$ from ref. [32], for lattice A_1.

A_1 as a function of $\tau = z_0/T$, at fixed $x_0 = 5a$, $y_0 = 11a$. The quark mass is $am = 0.0015$. There is a clear signal near $\tau = 0$. However, the temporal dependence does not seem to be as pronounced as expected from NLO χPT. The pattern is similar for the lattice A_2.

An interesting combination to consider is the product $R_\nu^+ R_\nu^-$, since NLO corrections cancel in this quantity (cf. eq. (2.39)). Writing the weak LECs as

$$g_1^\pm = [g_1^\pm]^{\rm bare}\, \frac{k_1^\pm Z_{11}^\pm}{Z_A^2}\,, \tag{3.10}$$

eqs. (2.39) and (2.41) imply that we may expect:

$$R_\nu^+ R_\nu^- = [g_1^+ g_1^-]^{\rm bare} \left(1 - \frac{1}{|\nu|^2}\right) + \dots\,. \tag{3.11}$$

The results for the lattice A_1 are shown in Fig. 9. A constant fit around $z_0 = 0$, followed by a chiral extrapolation in each topological sector, gives the values shown in Table 5. The agreement with the result obtained from the left-current three-point functions [17] is quite good. Note that the renormalization factors for the lattice A_1 are the same as those in ref. [17] and therefore the bare couplings can be compared directly. Those for the lattice A_2 have not been evaluated. However, the difference is expected to be well below the statistical uncertainty. Indeed a LO computation in bare perturbation theory yields variations at the 1–2% level, and the results of ref. [23] indicate that this perturbative estimate is realistic.

In order to then estimate $[g_1^+]^{\rm bare}$ and $[g_1^-]^{\rm bare}$ individually, we consider the following fits of the LMA data:

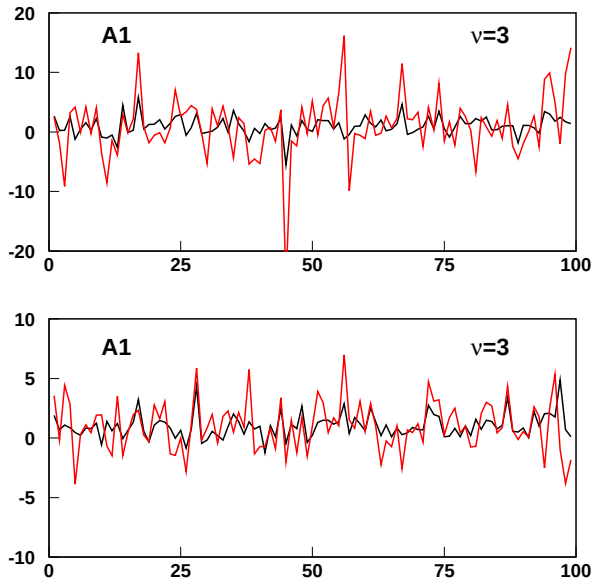

Figure 6: The Monte Carlo history of the three-point correlators $\bar{A}_\nu - \tilde{A}_\nu$ (top) and $\bar{A}_\nu + \tilde{A}_\nu$ (bottom), at $z_0 = 0$, normalized to the average, on the lattice A_1, for $|\nu| = 3$ and $am = 0.0015$. The dark line corresponds to the LMA and the light one to the non-LMA amplitude.

$\lvert\nu\rvert$	$[g_1^+ g_1^-]^{\rm bare}$ (A_1)	$[g_1^+ g_1^-]^{\rm bare}$ (A_2)	$[g_1^+ g_1^-]^{\rm bare}$ [17]
2	0.73(53)	0.72(39)	
3	0.94(20)	1.10(34)	
4	1.37(20)	1.60(36)	
5	1.64(20)	1.50(17)	
w.a. ($\lvert\nu\rvert > 2$)	1.32(11)	1.45(14)	1.47(12)
χ^2/d.o.f.	3.1	0.7	

Table 5: Values of the product of the bare couplings obtained from fits to a constant in the time interval $|z_0| \leq a$ for lattice A_1 and $|z_0| \leq 2a$ for A_2. The last row shows the weighted averages (w.a) over topological sectors $|\nu| > 2$ for the two lattices and also the result obtained in ref. [17] with a different method.

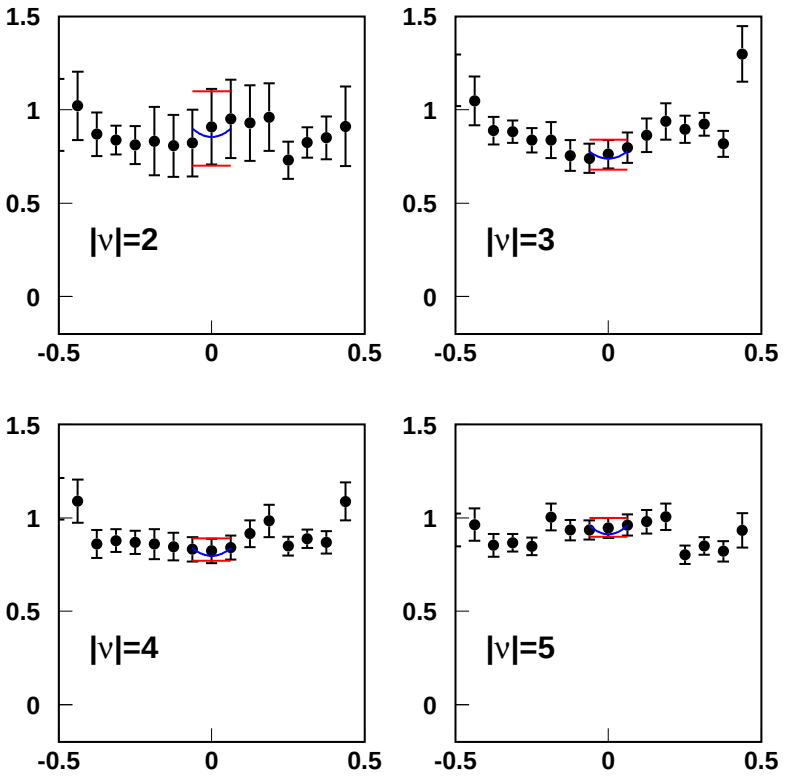

Figure 7: $R_\nu^+/(1-1/|\nu|)$ in different topological sectors for the lattice A_1 as a function of z_0/T for fixed $x_0 = 5a$, $y_0 = 11a$, at the smallest quark mass $am = 0.0015$. The horizontal lines represent the 1σ boundaries of a LO fit, while the curved line is the best NLO fit.

Fit A. At LO we expect (cf. eq. (2.39))

$$R_\nu^\pm = [g_1^\pm]^{\rm bare}\left(1 \mp \frac{1}{|\nu|}\right) , \tag{3.12}$$

therefore we fit $R_\nu^\pm / \left(1 \mp \frac{1}{|\nu|}\right)$ to a constant around $z_0 = 0$. The results are shown as the bands in Figs. 7, 8.

The results for the bare couplings are listed in Table 6. The results on the lattices A_1 and A_2 are again perfectly compatible, which implies that scaling violations are well below the statistical uncertaintities. There is a significant difference with the $[g_1^\pm]^{\rm bare}$ obtained from a LO matching of left-current three-point functions in ref. [17]: while our $[g_1^-]^{\rm bare}$ is smaller, our $[g_1^+]^{\rm bare}$ is larger. This is, however, not unexpected, given that chiral corrections tend to

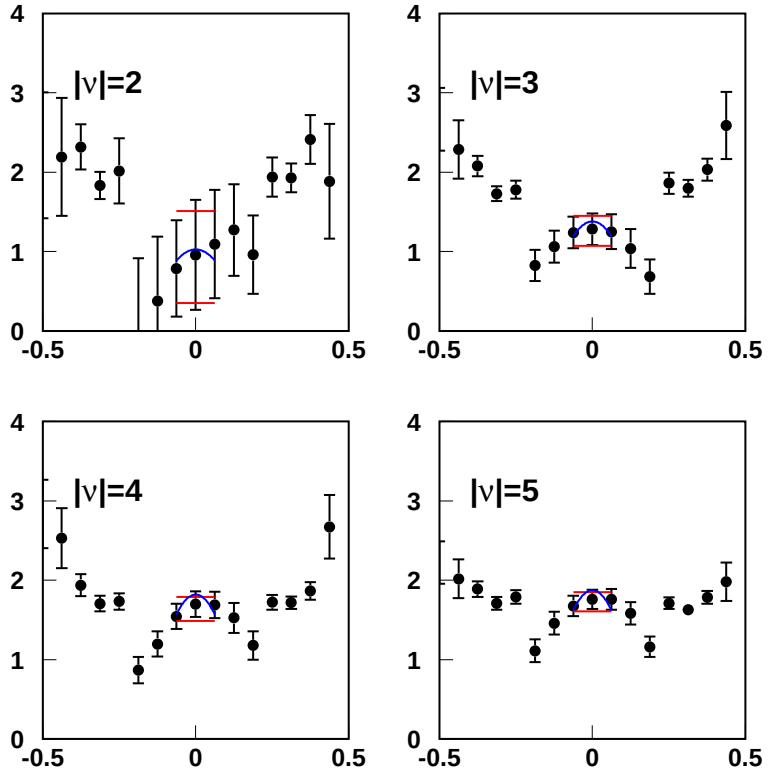

Figure 8: $R_\nu^-/(1+1/|\nu|)$ in different topological sectors for the lattice A_1 as a function of z_0/T for fixed $x_0 = 5a$, $y_0 = 11a$, at the smallest quark mass $am = 0.0015$. The horizontal lines represent the 1σ boundaries of a LO fit, while the curved line is the best NLO fit.

decrease $[g_1^-]^{\rm bare}$ and increase $[g_1^+]^{\rm bare}$ in ref. [17], and do the opposite in the present work.

Fit B. At NLO we expect (cf. eq. (2.39))

$$R_\nu^\pm = [g_1^\pm]^{\rm bare}\left(1 \mp \frac{1}{|\nu|}\right)\left[1 \pm r_\pm^q(z_0)\right] . \tag{3.13}$$

Numerical values of $(FL)^2 r_\pm^q(z_0)$ for small z_0 are shown in Table 7. Taking a value $FL \sim 1.1$, the NLO prediction gives a stronger temporal dependence than that seen in the data. The fits have a bad χ^2 if more that 3(5) points are included for lattice $A_1(A_2)$. This already indicates that NNLO could be significant. With so few points it does not make sense to do a two parameter fit, leaving the normalization of the NLO correction free, because there is

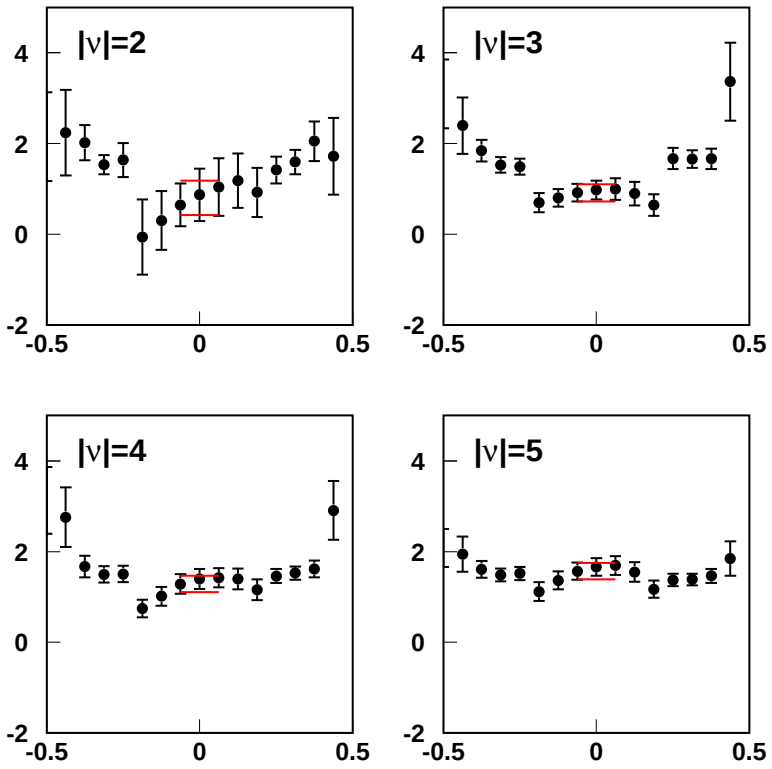

Figure 9: $R_\nu^+ R_\nu^- / (1 - 1/\nu^2)$ in different topological sectors on the lattice A_1 as a function of z_0/T for fixed $x_0 = 5a$, $y_0 = 11a$, at the smallest quark mass $am = 0.0015$. The bands represent the 1σ fits to a constant.

not much curvature in the data. Therefore we fix $(FL)^2 = 1.14 - 1.40$, corresponding to the range of values obtained from fitting various two-point functions here and in ref. [33]. We then perform linear one-parameter fits for $[g_1^\pm]^{\rm bare}$. The results are summarized in Table 8.

The results obtained for $[g_1^\pm]^{\rm bare}$ on the lattices A_1 and A_2 are again fully compatible, indicating small scaling violations. However, the effect of a 10% uncertainty in F results in a significant systematic uncertainty especially in $[g_1^-]^{\rm bare}$, which is much more sensitive to NLO corrections. In fact the difference between the results for $[g_1^-]^{\rm bare}$ obtained from LO and NLO matchings is too large for even the latter results to be trustworthy.

A comparison with the results of a NLO matching in ref. [17] shows that $[g_1^+]^{\rm bare}$ is in rather good agreement. This is quite non-trivial, given the very different NLO chiral corrections in the two cases, and could be an indication that NNLO corrections are not very important for

	$[g_1^-]^{\rm bare}$			$[g_1^+]^{\rm bare}$		
$\|\nu\|$	A_1	A_2	[17]	A_1	A_2	[17]
1	3.1(1.6)					
2	0.8(7)	1.7(0.7)		0.9(2)	0.44(13)	
3	1.2(2)	1.46(35)		0.76(8)	0.80(10)	
4	1.65(15)	1.85(31)		0.83(6)	0.89(10)	
5	1.73(12)	1.74(15)		0.95(5)	0.86(6)	
w.a. ($\|\nu\| > 2$)	1.60(8)	1.72(13)	2.42(13)	0.87(3)	0.85(5)	0.60(4)
χ^2/d.o.f.	2.6	0.4		2.4	0.2	

Table 6: Values of the bare couplings obtained from a LO fit in the time interval $|z_0| \leq a$ on lattice A_1 and $|z_0| \leq 2a$ on lattice A_2.

z_0	$[(FL)^2 r_\pm^q(z_0)]_{A_1}$	$[(FL)^2 r_\pm^q(z_0)]_{A_2}$
0	0.62839	0.58270
a	0.73420	0.61454
$2a$	1.23214	0.72759

Table 7: Values of $(FL)^2 r_\pm^q(z_0)$ for $z_0 = 0, a, 2a$, with $x_0 = 5a$, $y_0 = 11a$ for lattice A_1 and $x_0 = 8a$, $y_0 = 16a$ for lattice A_2.

this quantity. On the other hand, our $[g_1^-]^{\rm bare}$ lies significantly above the result of ref. [17], but this could be accounted for by an effect of 30% in the NNLO corrections, which does not appear unreasonable, given that the size of the NLO corrections is 50 – 60%. It is interesting to note, however, that due to the fact that the there is a cancellation between the LO and NLO terms in R_ν^-, the uncertainty in the NLO corrections has a bigger relative impact in the determination of $[g_1^-]^{\rm bare}$ than in $[g_1^+]^{\rm bare}$.

Obviously it is necessary to bring this systematic error under control, which can only be achieved by going to larger volumes and performing a detailed finite-size scaling study. Given that this is a quenched exploratory study and that going to larger volumes in the quenched approximation is no guarantee of success, we will not pursue this further here. We will consider, however, alternative estimates of $[g_1^-]^{\rm bare}$ that could be less affected by higher order

	$[g_1^-]^{\rm bare}$		
$\lvert\nu\rvert$	A_1	A_2	[17]
2	2(2) – 1.6(1.4)	4(2) – 3(1)	
3	3.1(5) – 2.5(4)	3.4(8) – 2.7(7)	
4	4.2(4) – 3.3(3)	4.3(7) – 3.5(6)	
5	4.4(3) – 3.4(2)	4.0(4) – 3.2(3)	
w.a. ($\lvert\nu\rvert > 2$)	4.1(2) – 3.2(2)	4.0(3) – 3.2(3)	2.33(11)
χ^2/d.o.f.	2.5 – 2.0	0.4 – 0.4	

	$[g_1^+]^{\rm bare}$		
$\lvert\nu\rvert$	A_1	A_2	[17]
2	0.56(13) – 0.60(14)	0.30(9) – 0.32(10)	
3	0.47(5) – 0.51(5)	0.53(7) – 0.57(7)	
4	0.52(4) – 0.55(4)	0.59(7) – 0.63(7)	
5	0.59(3) – 0.63(3)	0.55(4) – 0.59(4)	
w.a. ($\lvert\nu\rvert > 2$)	0.55(2) – 0.58(2)	0.57(4) – 0.61(4)	0.63(4)
χ^2/d.o.f.	2.4 – 2.6	0.3 – 0.2	

Table 8: Values of the bare couplings obtained from a NLO fit in the interval $|z_0| \leq a$. The ranges indicated correspond to considering $(FL)^2 = 1.14 - 1.40$.

corrections.

One possible strategy[5] is to obtain $[g_1^-]^{\rm bare}$ indirectly from $[g_1^+ g_1^-]^{\rm bare}$ and $[g_1^+]^{\rm bare}$. The first quantity is extracted from the product $R_\nu^+ R_\nu^-$ where the NLO correction vanishes, while the second quantity is extracted from R_ν^+, where the NLO contribution has the same sign as the LO, and therefore the uncertainty due to higher order effects is less relevant on relative terms. The results of such an approach are summarized in Table 9. The results for $[g_1^-]^{\rm bare}$ are now very close to those in ref. [17], and are significantly less sensitive to the uncertainty in F, as expected.

Alternatively, as is clear from Table 1, on could decrease the chiral corrections very signifi-

[5]This was the strategy followed in ref. [17].

	$[g_1^-]^{\rm bare}$		
$\lvert\nu\rvert$	A_1	A_2	[17]
2	1.3(1.1) – 1.2(1.0)	2.4(1.1) – 2.2(1.0)	
3	1.99(32) – 1.85(30)	2.1(5) – 1.9(5)	
4	2.66(24) – 2.47(22)	2.71(45)– 2.54(42)	
5	2.79(19) – 2.60(18)	2.65(24) – 2.48(22)	
w.a. ($\lvert\nu\rvert > 2$)	2.61(14) – 2.42(13)	2.58(20) – 2.42(18)	2.33(11)
χ^2/d.o.f.	2.3 – 2.3	0.5 – 0.6	

Table 9: Value of the bare coupling $[g_1^-]^{\rm bare}$ obtained from a NLO fit of $R_\nu^+ R_\nu^-$ and R_ν^+ in the interval $|z_0| \leq a$ for lattices A_1 and A_2. The ranges indicated correspond to considering $(FL)^2 = 1.14 - 1.40$.

cantly by increasing the distances τ_x and τ_y between the pseudoscalar densities and the weak operator, at the expense of decreasing $|\tau_x - \tau_y|$. Note that chiral corrections (up to NLO) are in fact insensitive to the last separation. In principle, the distance between the pseudoscalar sources has to be large enough compared with the cutoff and the physical distance scales of QCD. However it is an empirical observation that two-point functions approach the asymptotic behaviour very fast in the ϵ-regime, and we are therefore confident that it makes sense to investigate the three-point functions for larger values of τ_x and τ_y, even on a lattice as small as $T = 16a$. Provided the effects of higher scales can be neglected, choosing $x_0 = 7a$ and $y_0 = 9a$ on the lattice A_1 can reduce the chiral corrections by 30%. The results obtained for this choice are summarized in Table 10.

A few observations are in order. The changes in $[g_1^+]^{\rm bare}$ and $[g_1^+ g_1^-]^{\rm bare}$ with respect to the case $\tau_x \simeq \tau_y \simeq |\tau_x - \tau_y|$ are quite small, but the change in $[g_1^-]^{\rm bare}$ is very significant (yet still at the level expected from NNLO chiral corrections), bringing the value of $[g_1^-]^{\rm bare}$ to agreement with that from the indirect determination, and with that of ref. [17]. The χ^2/d.o.f. of the fits get improved and the effect of the uncertainty in F on $[g_1^-]^{\rm bare}$ gets reduced to the level of 10%. In general the agreement of these results with those of ref. [17] is quite remarkable. Unfortunately the distance between the sources is too small to be confident that the effect of higher scales is negligible, but these results provide further evidence that the discrepancy between the different determinations of $[g_1^-]^{\rm bare}$ can indeed be ascribed to higher order chiral corrections.

$\lvert\nu\rvert$	$[g_1^-]^{\rm bare}$	$[g_1^+]^{\rm bare}$	$[g_1^+ g_1^-]^{\rm bare}$
2	5.5(2.7) – 4.9(2.4)	0.56(14) – 0.59(14)	2.5(1.3)
3	3.45(54) – 3.10(48)	0.59(7) – 0.62(7)	1.73(35)
4	2.75(31) – 2.46(28)	0.62(5) – 0.65(5)	1.47(23)
5	2.62(13) – 2.36(12)	0.66(4) – 0.69(4)	1.47(12)
w.a. ($\lvert\nu\rvert > 2$)	2.68(11) – 2.41(11)	0.63(3) – 0.66(3)	1.49(10)
χ^2/d.o.f.	1.1	0.45	0.25

Table 10: Values of the bare couplings obtained from a NLO fit in the interval $|z_0| \leq a$ for lattice A_1 and $x_0 = 7a$, $y_0 = 9a$. The ranges indicated correspond to considering $(FL)^2 = 1.14 - 1.40$.

4. Conclusions

The purpose of this paper has been to estimate the weak low-energy couplings $g_1^{\pm}$, defined in eq. (2.5), in the SU(4) chiral limit. Our method has been to measure the topological zero-mode contributions to three-point correlation functions of two pseudoscalar densities and a weak operator in sectors of non-trivial topology. The results of the measurements have been matched to NLO predictions of ϵ-regime chiral perturbation theory.

We have considered several fitting strategies for estimating the couplings g_1^+ and g_1^-, in an attempt to quantify the uncertainty induced by unknown higher order chiral corrections (NNLO), which are expected to be significant at the volume we have considered. While we observe small variations in the determination of g_1^+, as well as in the product $g_1^+ g_1^-$, between the different methods, the value of g_1^- seems to be significantly affected by higher orders.

Taking the bare couplings $[g_1^+]^{\rm bare}$ and $[g_1^+ g_1^-]^{\rm bare}$ cited in Table 8 for the lattice A_1, and the same renormalization factors and Wilson coefficients that were used in ref. [17], and inserting everything into eq. (3.10), we obtain

$$g_1^+ \simeq 0.46(5) \ , \quad g_1^+ g_1^- \simeq 1.2(2) \ . \tag{4.1}$$

The errors shown involve statistical uncertainties as well as the uncertainty from the determination of the (quenched) pion decay constant F. We have checked that discretization effects in these numbers are small. However, systematic errors related to higher order chiral corrections as well as the quenched approximation have not been quantified. In any case, both quantities are in good agreement with those of ref. [17], where they were extracted from observables with very different chiral corrections, so this is a strong indication that higher order chiral corrections could be under control.

The situation with g_1^- is less clear. The different fitting strategies we have explored give

values that differ by up to 30%, which is also the naive expectation for the magnitude of higher order chiral corrections. We have argued that an indirect extraction of g_1^- from the combinations in eq. (4.1) is the method that should be least sensitive to the uncertainty induced by higher orders. With this approach, we obtain from the results of Table 9

$$g_1^- \simeq 2.8(4) \ , \tag{4.2}$$

which is also in good agreement with the result of ref. [17]. We should stress however that we have seen evidence that higher order corrections could be significant for this quantity; the corresponding systematic error cannot be quantified precisely, and has not been included in eq. (4.2). Probably an error of 30% in eq. (4.2) would be a reasonable estimate.

The conclusions concerning the $\Delta I = 1/2$ rule are the same as in ref. [17]: there is a significant $\Delta I = 1/2$ enhancement already in the SU(4) limit, which cannot be explained by penguin dominance. However, this enhancement is not as large as the experimental one.

The method of the present study and that in refs. [16, 17] can be compared on two accounts. First of all, there is the issue of how well chiral perturbation theory converges with a given box size and geometry. In a symmetric box of size $(FL)^2 = 1.1$, for instance, the magnitude of next-to-leading order corrections in the method of refs. [16, 17] is $\sim 15\%$ (cf. Fig. 2 of ref. [16]), while in the present observables it is $\sim 60\%$ (cf. Table 1). In the present case the magnitude of the corrections can be reduced very significantly by taking the sources further away from the weak operator, while in the method of refs. [16, 17] this has no effect. Nevertheless, it could be concluded that from the point of view of chiral perturbation theory, the method of refs. [16, 17] appears to be preferable.

The second comparison concerns the numerical cost of the measurements carried out. On this account, on the contrary, the present method appears to be preferable: a good statistical signal could be achieved with significantly less computational effort than in ref. [17]. Indeed, the number of quark propagators required per quark mass to construct the observables is a factor of 5 smaller in the present work. Note also that this factor scales with $N_{\rm low}$, which is expected to scale with the volume[6].

These two competing aspects probably mean that, moving towards SU(3) symmetry and unquenched simulations, it would be wise to continue to probe the weak low-energy constants with (at least) two independent methods. In particular, the fact that chiral corrections are very different in the two cases, offers a good way of quantifying the systematics associated with the chiral fits. On the other hand, particularly in the SU(3) case where the penguin contractions need to be evaluated, which entails a significant numerical cost, it may be that the method introduced in the present work becomes preferable.

[6] A new method to solve the V^2-problem of low-mode preconditioning has been presented in ref. [34], and in principle could also be applied to low-mode averaging.

Acknowledgments

We wish to thank L. Giusti, M. Lüscher and P. Weisz for the joint development of important parts of the computer code used in this work. We acknowledge the computer resources provided by IBM MareNostrum at the BSC, the IBM Regatta at FZ Jülich and the PC-clusters at University of Valencia. P.H. and E.T. acknowledge partial financial support from the research grants FPA-2004-00996, FPA-2007-01678, FLAVIAnet and HA2005-0120. C.P. acknowledges financial support from the Ramón y Cajal programme, as well as the research grant FPA2006-05807. C.P. and P. H. acknowledge support from the Consolider-Ingenio 2010 Programme CPAN (CSD2007-00042).

Appendix A. Graph-by-graph results for the two-point correlator

For completeness, we present in this appendix graph-by-graph results for the two-point correlation function defined in eq. (2.22).

As usual, the Goldstone field is factorised into non-zero and zero-mode parts:

$$U(x) \equiv U_\xi(x)\, U_0 \ , \quad U_\xi(x) \equiv \exp\left[\frac{2i\xi(x)}{F}\right] . \tag{A.1}$$

The propagator of the non-zero modes ξ, which are perturbative, is of the form

$$\langle \xi_{ij}(x)\, \xi_{kl}(y)\rangle = \frac{1}{2}\Big[\delta_{il}\delta_{jk}G(x-y) - \delta_{ij}\delta_{kl}E(x-y)\Big] . \tag{A.2}$$

Here $G(x)$ is the massless non-zero mode propagator,

$$G(x) \equiv \frac{1}{V}\sum_{n\in\mathbb{Z}^4}\Big(1-\delta^{(4)}_{n,0}\Big)\frac{e^{ip\cdot x}}{p^2} \ , \quad V \equiv TL_1L_2L_3 \ , \quad p_0 \equiv \frac{2\pi n_0}{T} \ , \quad p_i \equiv \frac{2\pi n_i}{L_i} \ , \tag{A.3}$$

while $E(x)$ is the "trace part" whose form is affected by quenching; in the unquenched case it reads $E(x) = G(x)/N_{\rm f}$, while in the quenched case,

$$E(x) \equiv \frac{\alpha}{2N_c}G(x) + \frac{m_0^2}{2N_c}F(x) \ , \tag{A.4}$$

where

$$F(x) = \frac{1}{V}\sum_{n\in\mathbb{Z}^4}\Big(1-\delta^{(4)}_{n,0}\Big)\frac{e^{ip\cdot x}}{p^4} \ . \tag{A.5}$$

Since the zero-mode field U_0 is an x-independent constant, and we are only interested in contributions to the correlation function $\langle \mathcal{P}^a(x)\mathcal{L}_0^b(z)\rangle_\nu$ that remain non-zero after taking the derivative ∂_{x_0}, it is clear that the only graphs that can contribute are those where the two operators are connected by a non-zero mode propagator. Denoting the operator $\mathcal{P}^a$ by an open square; the operator $\mathcal{L}_0^b$ by an open half circle; the propagator in eq. (A.2) by a solid

line; the mass term in the chiral Lagrangian by a closed circle; the mass term originating from the Haar measure by a cross; $\mu \equiv m\Sigma V$; and choosing to list the results before taking the spatial average, time derivative, and zero-mass limit in eq. (2.22), we are led to:

$$= \frac{i\Sigma}{2}\partial_0 G(z-x)\Big\langle \mathrm{Tr}\left[(U_0 T^a + T^a U_0^\dagger)T^b\right]\Big\rangle\,, \tag{A.6}$$

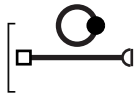

$$= -\frac{i\mu\Sigma}{4F^2}[N_{\rm f}G(0) - E(0)]\partial_0 G(z-x)\times$$
$$\times\Big[\Big\langle \mathrm{Tr}\left[(U_0 T^a + T^a U_0^\dagger)T^b\right]\mathrm{Tr}\left[U_0 + U_0^\dagger\right]\Big\rangle$$
$$-\Big\langle \mathrm{Tr}\left[(U_0 T^a + T^a U_0^\dagger)T^b\right]\Big\rangle\Big\langle \mathrm{Tr}\left[U_0 + U_0^\dagger\right]\Big\rangle\Big]\,, \tag{A.7}$$

$$= -\frac{iN_{\rm f}\Sigma}{3F^2V}\int_s \partial_0 G(z-s)G(s-x)\Big\langle \mathrm{Tr}\left[(U_0 T^a + T^a U_0^\dagger)T^b\right]\Big\rangle\,, \tag{A.8}$$

$$= -\frac{im\Sigma^2}{4F^2}\int_s \partial_0 G(z-s)G(s-x)\times$$
$$\times\Big\langle \mathrm{Tr}\left[(U_0 T^a + T^a U_0^\dagger)\{U_0 + U_0^\dagger, T^b\}\right]\Big\rangle$$
$$+\frac{im\Sigma^2}{2F^2}\int_s \partial_0 G(z-s)E(s-x)\times$$
$$\times\Big\langle \mathrm{Tr}\left[U_0 T^a + T^a U_0^\dagger\right]\mathrm{Tr}\left[T^b(U_0 + U_0^\dagger)\right]\Big\rangle\,, \tag{A.9}$$

$$= -\frac{iN_{\rm f}\Sigma}{6F^2}\Big[\partial_\nu^2 G(0)\int_s \partial_0 G(z-s)G(s-x) \tag{A.10}$$
$$+G(0)\int_s \partial_0\partial_\nu G(z-s)\partial_\nu G(s-x)\Big]\Big\langle \mathrm{Tr}\left[(U_0 T^a + T^a U_0^\dagger)T^b\right]\Big\rangle\,,$$

$$= 0\,, \tag{A.11}$$

$$= -\frac{iN_{\rm f}\Sigma}{3F^2}G(0)\partial_0 G(z-x)\Big\langle \mathrm{Tr}\left[(U_0 T^a + T^a U_0^\dagger)T^b\right]\Big\rangle\,, \tag{A.12}$$

$$= -\frac{i\Sigma}{3F^2}\Big[N_{\rm f}G(0) - \frac{3}{2}E(0)\Big]\partial_0 G(z-x)\times$$
$$\times\Big\langle \mathrm{Tr}\left[(U_0 T^a + T^a U_0^\dagger)T^b\right]\Big\rangle\,. \tag{A.13}$$

In the quenched case, there are two additional contributions, discussed around eqs. (2.27), (2.28):

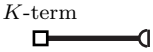

$$= \frac{2i\nu K N_{\rm c}}{m_0^2 FV}\partial_0 G(z-x)\times\Big\langle \mathrm{Tr}\left[(U_0 T^a - T^a U_0^\dagger)T^b\right]\Big\rangle\,, \tag{A.14}$$

$$\Big[\ \Big]_{K\text{-weight,conn.}} = \frac{i\nu m\Sigma K N_{\rm c}}{m_0^2 F}\partial_0 G(z-x)\times$$
$$\times\Big[\Big\langle \mathrm{Tr}\left[(U_0T^a+T^aU_0^\dagger)T^b\right]\mathrm{Tr}\,(U_0-U_0^\dagger)\Big\rangle$$
$$-\Big\langle \mathrm{Tr}\left[(U_0T^a+T^aU_0^\dagger)T^b\right]\Big\rangle\Big\langle \mathrm{Tr}\,(U_0-U_0^\dagger)\Big\rangle\Big]\ . \qquad (A.15)$$

Here we made use of the fact that the integral over the zero-mode of the singlet field, Φ_0, is Gaussian, and Φ_0 can be approximated by the corresponding saddle point value,

$$\Phi_0 = -2i\frac{\nu N_{\rm c}}{m_0^2 FV}\ . \qquad (A.16)$$

In fact this value was already inserted in order to arrive at the K-term of eq. (2.28).

As far as the zero-mode integrals appearing in eqs. (A.6)–(A.13) are concerned, the general trick to use is that, because of the invariance of the integration measure,

$$\langle A_{ij}\,B_{kl}\rangle = c_1\,\delta_{ij}\delta_{kl} + c_2\,\delta_{il}\delta_{jk}\ , \qquad (A.17)$$

where $A, B \in \{U_0, U_0^\dagger\}$. Carrying out contractions and solving the quadratic system yields

$$c_1 = \frac{1}{N_{\rm f}(N_{\rm f}^2-1)}\Big\{N_{\rm f}\langle \mathrm{Tr}\,[A]\ \mathrm{Tr}\,[B]\rangle - \langle \mathrm{Tr}\,[A\,B]\rangle\Big\}\ , \qquad (A.18)$$

$$c_2 = \frac{1}{N_{\rm f}(N_{\rm f}^2-1)}\Big\{N_{\rm f}\langle \mathrm{Tr}\,[A\,B]\rangle - \langle \mathrm{Tr}\,[A]\ \mathrm{Tr}\,[B]\rangle\Big\}\ . \qquad (A.19)$$

This leads to integrals whose values are listed in appendix B of ref. [21]. For the zero-mass limit in eq. (2.22) we only need the poles in $1/\mu^n$, which are also listed in ref. [21].

Applying this recipe in practice, we obtain

$$\lim_{m\to 0}(mV\Sigma)\Big\langle \mathrm{Tr}\left[(U_0T^a+T^aU_0^\dagger)T^b\right]\Big\rangle = 2|\nu|\mathrm{Tr}\,[T^aT^b]\ , \qquad (A.20)$$

$$\lim_{m\to 0}(mV\Sigma)^2\Big[\Big\langle \mathrm{Tr}\,[(U_0T^a+T^aU_0^\dagger)T^b]\mathrm{Tr}\,[U_0+U_0^\dagger]\Big\rangle$$
$$-\Big\langle \mathrm{Tr}\,[(U_0T^a+T^aU_0^\dagger)T^b]\Big\rangle\Big\langle \mathrm{Tr}\,[U_0+U_0^\dagger]\Big\rangle\Big] = -4|\nu|\mathrm{Tr}\,[T^aT^b]\ , \qquad (A.21)$$

$$\lim_{m\to 0}(mV\Sigma)^2\Big\langle \mathrm{Tr}\left[(U_0T^a+T^aU_0^\dagger)\{U_0+U_0^\dagger,T^b\}\right]\Big\rangle = 4|\nu|(2|\nu|-N_{\rm f})\mathrm{Tr}\,[T^aT^b]\ , \qquad (A.22)$$

$$\lim_{m\to 0}(mV\Sigma)^2\Big\langle \mathrm{Tr}\left[U_0T^a+T^aU_0^\dagger\right]\mathrm{Tr}\left[T^b(U_0+U_0^\dagger)\right]\Big\rangle = -4|\nu|\mathrm{Tr}\,[T^aT^b]\ . \qquad (A.23)$$

The additional integrals needed in the quenched case (eqs. (A.14), (A.15)) read

$$\lim_{m\to 0}(mV\Sigma)\Big\langle \mathrm{Tr}\left[(U_0T^a-T^aU_0^\dagger)T^b\right]\Big\rangle = -2\nu\,\mathrm{Tr}\,[T^aT^b]\ , \qquad (A.24)$$

$$\lim_{m\to 0}(mV\Sigma)^2\Big[\Big\langle \mathrm{Tr}\,[(U_0T^a+T^aU_0^\dagger)T^b]\mathrm{Tr}\,[U_0-U_0^\dagger]\Big\rangle$$
$$-\Big\langle \mathrm{Tr}\,[(U_0T^a+T^aU_0^\dagger)T^b]\Big\rangle\Big\langle \mathrm{Tr}\,[U_0-U_0^\dagger]\Big\rangle\Big] = 4\nu\,\mathrm{Tr}\,[T^aT^b]\ . \qquad (A.25)$$

Inserting the last two into eqs. (A.14), (A.15), we see immediately that the two quenched terms cancel against each other.

Let us finally consider the spacetime dependence. After taking the spatial average and time derivative in eq. (2.22), omitting contact terms, and denoting $\tau_x = (x_0 - z_0)/T$, we get

$$\partial_{x_0} \int_{\mathbf{x}} \partial_0 G(z-x) \;=\; -\frac{1}{T}\,, \tag{A.26}$$

$$\partial_{x_0} \int_{\mathbf{x}} \int_s \partial_0 G(z-s) G(s-x) \;=\; T h_1(\tau_x)\,, \tag{A.27}$$

$$\partial_{x_0} \int_{\mathbf{x}} \int_s \partial_0 \partial_\nu G(z-s) \partial_\nu G(s-x) \;=\; \frac{1}{T}\,, \tag{A.28}$$

where the function $h_1(\tau)$ is given in eq. (2.26). In dimensional regularization, the object $\partial_\nu^2 G(0)$ appearing in eq. (A.10) evaluates to $\partial_\nu^2 G(0) = 1/V$. On the other hand, the constants $G(0), E(0)$, appearing in several contributions, cancel completely in the final result.

Summing now all the results together, but making no assumptions about the form of $E(x)$, and expressing the result as in eq. (2.22), we obtain

$$\mathcal{B}_\nu(x_0 - z_0) = \frac{|\nu|}{T}\biggl[1 + \frac{2|\nu|T^2}{F^2 V} h_1(\tau_x) + \frac{2T}{F^2 V} \partial_{x_0} \int_{\mathbf{x}} \int_s \partial_0 G(z-s) E(s-x)\biggr]\,. \tag{A.29}$$

Appendix B. Graph-by-graph results for the three-point correlator

For completeness, we present in this appendix graph-by-graph results for the three-point correlation function defined in eq. (2.30). To be precise, we list results for the operator $\mathcal{O}_{rsuv}$ from eq. (2.32), with r, s, u, v assumed to be all different; results for the operator $\mathcal{O}_1$ are then obtained by symmetrizing according to eq. (2.31).

Since the zero-mode field U_0 is an x-independent constant, and we are only interested in contributions to the correlation function $-\langle \mathcal{P}^a(x) \mathcal{O}_{rsuv}(z) \mathcal{P}^b(y)\rangle_\nu$ that remain non-zero after taking the derivatives $\partial_{x_0}\partial_{y_0}$, it is clear that the only graphs that can contribute are those where the pseudoscalar densities are connected to each other or to the weak operator by non-zero mode propagators. Furthermore, in the SU(4) limit we can assume all the indices r, s, u, v to be different, which allows us to omit structures like $\delta_{ur}, \delta_{us}, \delta_{vr}, \delta_{vs}$; this means that the weak operator needs to be connected to at least one of the pseudoscalar densities. Denoting the operator $\mathcal{P}^a$ by an open square; the operator $\mathcal{O}_{rsuv}$ by an open circle; the propagator in eq. (A.2) by a solid line; and choosing to list the results before taking the spatial averages, time derivatives, and zero-mass limit in eq. (2.30), we are led to:

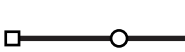

$$\begin{aligned} &= \frac{\Sigma^2}{4} \partial_\mu G(x-z) \partial_\mu G(y-z) \times \\ &\quad \times \biggl[\Bigl\langle (U_0 T^a + T^a U_0^\dagger)_{ur} (U_0 T^b + T^b U_0^\dagger)_{vs} \Bigr\rangle + (a \leftrightarrow b)\biggr]\,, \end{aligned} \tag{B.1}$$

$$= \frac{\mu\Sigma^2}{8F^2}[N_{\rm f}G(0)-E(0)]\partial_\mu G(x-z)\partial_\mu G(y-z)\times$$
$$\times\Big[\Big\langle(U_0T^a+T^aU_0^\dagger)_{ur}(U_0T^b+T^bU_0^\dagger)_{vs}\Big\rangle\Big\langle{\rm Tr}\,(U_0+U_0^\dagger)\Big\rangle$$
$$-\Big\langle(U_0T^a+T^aU_0^\dagger)_{ur}(U_0T^b+T^bU_0^\dagger)_{vs}{\rm Tr}\,(U_0+U_0^\dagger)\Big\rangle$$
$$+(a\leftrightarrow b)\Big]\,, \qquad \text{(B.2)}$$

$$= -\frac{N_{\rm f}\Sigma^2}{6F^2V}\Big[\partial_\mu G(x-z)\int_s\partial_\mu G(y-s)G(s-z)+(x\leftrightarrow y)\Big]\times$$
$$\times\Big[\Big\langle(U_0T^a+T^aU_0^\dagger)_{ur}(U_0T^b+T^bU_0^\dagger)_{vs}\Big\rangle+(a\leftrightarrow b)\Big]\,, \qquad \text{(B.3)}$$

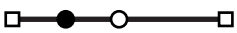

$$= -\frac{m\Sigma^3}{8F^2}\times\Big\{\partial_\mu G(x-z)\int_s\partial_\mu G(y-s)G(s-z)\times$$
$$\times\Big\langle(U_0T^a+T^aU_0^\dagger)_{ur}\{U_0+U_0^\dagger,U_0T^b+T^bU_0^\dagger\}_{vs}\Big\rangle$$
$$+\partial_\mu G(y-z)\int_s\partial_\mu G(x-s)G(s-z)\times$$
$$\times\Big\langle(U_0T^b+T^bU_0^\dagger)_{ur}\{U_0+U_0^\dagger,U_0T^a+T^aU_0^\dagger\}_{vs}\Big\rangle$$
$$-2\partial_\mu G(x-z)\int_s\partial_\mu E(y-s)G(s-z)\times$$
$$\times\Big\langle(U_0T^a+T^aU_0^\dagger)_{ur}(U_0+U_0^\dagger)_{vs}{\rm Tr}\,(U_0T^b+T^bU_0)\Big\rangle$$
$$-2\partial_\mu G(y-z)\int_s\partial_\mu E(x-s)G(s-z)\times$$
$$\times\Big\langle(U_0T^b+T^bU_0^\dagger)_{ur}(U_0+U_0^\dagger)_{vs}{\rm Tr}\,(U_0T^a+T^aU_0^\dagger)\Big\rangle$$
$$+(r\leftrightarrow s,u\leftrightarrow v)\Big\}\,, \qquad \text{(B.4)}$$

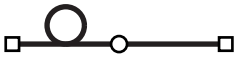

$$= -\frac{N_{\rm f}\Sigma^2}{12F^2}\Big[G(0)\partial_\mu G(x-z)\int_s\partial_\mu\partial_\nu G(y-s)\partial_\nu G(s-z)$$
$$+\partial_\nu^2G(0)\partial_\mu G(x-z)\int_s\partial_\mu G(y-s)G(s-z)+(x\leftrightarrow y)\Big]\times$$
$$\times\Big[\Big\langle(U_0T^a+T^aU_0^\dagger)_{ur}(U_0T^b+T^bU_0^\dagger)_{vs}\Big\rangle+(a\leftrightarrow b)\Big]\,, \qquad \text{(B.5)}$$

$$= -\frac{\Sigma^2}{12F^2}\int_s\Big[G(x-s)G(y-s)\partial_\mu\partial_\nu G(s-z)\partial_\mu\partial_\nu G(s-z)$$
$$+\partial_\nu G(x-s)G(y-s)\partial_\mu G(s-z)\partial_\mu\partial_\nu G(s-z)$$
$$+G(x-s)\partial_\nu G(y-s)\partial_\mu G(s-z)\partial_\mu\partial_\nu G(s-z)$$

$$+\partial_\nu G(x-s)\partial_\nu G(y-s)\partial_\mu G(s-z)\partial_\mu G(s-z)\Big] \times$$
$$\times\Big[\Big\langle (U_0T^a+T^aU_0^\dagger)_{us}(U_0T^b+T^bU_0^\dagger)_{vr}\Big\rangle + (a\leftrightarrow b)\Big]\,, \quad \text{(B.6)}$$

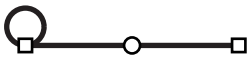

$$= \frac{\Sigma^2}{3F^2}\Big[\frac{3}{2}E(0)-N_{\rm f}G(0)\Big]\partial_\mu G(x-z)\partial_\mu G(y-z)\times$$
$$\times\Big[\Big\langle (U_0T^a+T^aU_0^\dagger)_{ur}(U_0T^b+T^bU_0^\dagger)_{vs}\Big\rangle + (a\leftrightarrow b)\Big]\,, \quad \text{(B.7)}$$

$$= -\frac{\Sigma^2}{12F^2}\Big\{G(x-y)\Big[\partial_\mu G(y-z)\Big]^2+(x\leftrightarrow y)\Big\}\times$$
$$\times\Big[\Big\langle (U_0T^a+T^aU_0^\dagger)_{us}(U_0T^b+T^bU_0^\dagger)_{vr}\Big\rangle + (a\leftrightarrow b)\Big]\,, \quad \text{(B.8)}$$

$$= -\frac{\Sigma^2}{4F^2}G(x-y)\partial_\mu G(x-z)\partial_\mu G(y-z)\times$$
$$\times\Big[\Big\langle (U_0T^a-T^aU_0^\dagger)_{us}(U_0T^b-T^bU_0^\dagger)_{vr}\Big\rangle + (a\leftrightarrow b)\Big]$$
$$+\frac{\Sigma^2}{2F^2}E(x-y)\partial_\mu G(x-z)\partial_\mu G(y-z)\times$$
$$\times\Big[\Big\langle (U_0T^a-T^aU_0^\dagger)_{ur}(U_0T^b-T^bU_0^\dagger)_{vs}\Big\rangle + (a\leftrightarrow b)\Big]\,, \quad \text{(B.9)}$$

$$= 0\,, \quad \text{(B.10)}$$

$$= 0\,, \quad \text{(B.11)}$$

$$= -\frac{\Sigma^2}{12F^2}\Big[\partial_\mu^2 G(0)G(x-z)G(y-z)$$
$$+3G(0)\partial_\mu G(x-z)\partial_\mu G(y-z)\Big]\times$$
$$\times\Big[\Big\langle (U_0T^a+T^aU_0^\dagger)_{us}(U_0T^b+T^bU_0^\dagger)_{vr}\Big\rangle + (a\leftrightarrow b)\Big]$$
$$-\frac{N_{\rm f}\Sigma^2}{3F^2}G(0)\partial_\mu G(x-z)\partial_\mu G(y-z)\times$$
$$\times\Big[\Big\langle (U_0T^a+T^aU_0^\dagger)_{ur}(U_0T^b+T^bU_0^\dagger)_{vs}\Big\rangle + (a\leftrightarrow b)\Big]\,. \quad \text{(B.12)}$$

In the quenched case, there are two additional contributions,

K-term 

$$= \frac{\nu\Sigma K N_{\rm c}}{m_0^2 FV}\,\partial_\mu G(x-z)\partial_\mu G(y-z)\times$$

$$\times\Big[\Big\langle (U_0T^a+T^aU_0^\dagger)_{ur}(U_0T^b-T^bU_0^\dagger)_{vs}\Big\rangle$$
$$+\Big\langle (U_0T^a+T^aU_0^\dagger)_{vs}(U_0T^b-T^bU_0^\dagger)_{ur}\Big\rangle$$
$$+(a\leftrightarrow b)\Big]\,, \tag{B.13}$$

$\Big[$ 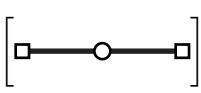 $\Big]_{K\text{-weight,conn.}}$

$$= \frac{\nu m\Sigma^2 K N_{\rm c}}{2m_0^2F}\,\partial_\mu G(x-z)\partial_\mu G(y-z)\times$$
$$\times\Big[\Big\langle (U_0T^a+T^aU_0^\dagger)_{ur}(U_0T^b+T^bU_0^\dagger)_{vs}{\rm Tr}\,(U_0-U_0^\dagger)\Big\rangle$$
$$-\Big\langle (U_0T^a+T^aU_0^\dagger)_{ur}(U_0T^b+T^bU_0^\dagger)_{vs}\Big\rangle\Big\langle {\rm Tr}\,(U_0-U_0^\dagger)\Big\rangle$$
$$+(a\leftrightarrow b)\Big]\,. \tag{B.14}$$

Employing the same trick as in eqs. (A.17)–(A.19), the zero-mode integrals become

$$\lim_{m\to 0}(mV\Sigma)^2\Big\{\Big\langle (U_0T^a+T^aU_0^\dagger)_{ur}(U_0T^b+T^bU_0^\dagger)_{vs}\Big\rangle+(a\leftrightarrow b)\Big\}$$
$$=4\Big[\nu^2T^{\{a}_{ur}T^{b\}}_{vs}-|\nu|T^{\{a}_{us}T^{b\}}_{vr}\Big]\,, \tag{B.15}$$
$$\lim_{m\to 0}(mV\Sigma)^2\Big\{\Big\langle (U_0T^a-T^aU_0^\dagger)_{ur}(U_0T^b-T^bU_0^\dagger)_{vs}\Big\rangle+(a\leftrightarrow b)\Big\}$$
$$=4\Big[\nu^2T^{\{a}_{ur}T^{b\}}_{vs}-|\nu|T^{\{a}_{us}T^{b\}}_{vr}\Big]\,, \tag{B.16}$$
$$\lim_{m\to 0}(mV\Sigma)^3\Big\{\Big\langle (U_0T^a+T^aU_0^\dagger)_{ur}(U_0T^b+T^bU_0^\dagger)_{vs}\Big\rangle\Big\langle {\rm Tr}\,(U_0+U_0^\dagger)\Big\rangle$$
$$-\Big\langle (U_0T^a+T^aU_0^\dagger)_{ur}(U_0T^b+T^bU_0^\dagger)_{vs}{\rm Tr}\,(U_0+U_0^\dagger)\Big\rangle+(a\leftrightarrow b)\Big\}$$
$$=16\Big[\nu^2T^{\{a}_{ur}T^{b\}}_{vs}-|\nu|T^{\{a}_{us}T^{b\}}_{vr}\Big]\,, \tag{B.17}$$
$$\lim_{m\to 0}(mV\Sigma)^3\Big\{\Big\langle (U_0T^a+T^aU_0^\dagger)_{ur}\{U_0+U_0^\dagger,U_0T^b+T^bU_0^\dagger\}_{vs}\Big\rangle+(r\leftrightarrow s,u\leftrightarrow v)\Big\}$$
$$=8\Big[(|\nu|-N_{\rm f}\nu^2+2\nu^2|\nu|)T^{\{a}_{ur}T^{b\}}_{vs}+(N_{\rm f}|\nu|-3\nu^2)T^{\{a}_{us}T^{b\}}_{vr}\Big]\,, \tag{B.18}$$
$$\lim_{m\to 0}(mV\Sigma)^3\Big\{\Big\langle (U_0T^a+T^aU_0^\dagger)_{ur}(U_0+U_0^\dagger)_{vs}{\rm Tr}\,(U_0T^b+T^bU_0^\dagger)\Big\rangle+(r\leftrightarrow s,u\leftrightarrow v)\Big\}$$
$$=8\Big[-\nu^2T^{\{a}_{ur}T^{b\}}_{vs}+|\nu|T^{\{a}_{us}T^{b\}}_{vr}\Big]\,, \tag{B.19}$$

where we again omitted all terms proportional to $\delta_{us},\delta_{ur},\delta_{vs},\delta_{vr}$.

The additional zero-mode integrals needed in the quenched case read

$$\lim_{m\to 0}(mV\Sigma)^2\Big\{\Big\langle (U_0T^a+T^aU_0^\dagger)_{ur}(U_0T^b-T^bU_0^\dagger)_{vs}\Big\rangle$$

$$+\Big\langle (U_0T^a + T^aU_0^\dagger)_{vs}(U_0T^b - T^bU_0^\dagger)_{ur}\Big\rangle + (a \leftrightarrow b)\Big\}$$
$$= -8\nu\Big[|\nu| T^{\{a}_{ur}T^{b\}}_{vs} - T^{\{a}_{us}T^{b\}}_{vr}\Big] \,, \tag{B.20}$$
$$\lim_{m\to 0}(mV\Sigma)^3\Big\{\Big\langle (U_0T^a + T^aU_0^\dagger)_{ur}(U_0T^b + T^bU_0^\dagger)_{vs}\mathrm{Tr}\,(U_0 - U_0^\dagger)\Big\rangle$$
$$-\Big\langle (U_0T^a + T^aU_0^\dagger)_{ur}(U_0T^b + T^bU_0^\dagger)_{vs}\Big\rangle\Big\langle \mathrm{Tr}\,(U_0 - U_0^\dagger)\Big\rangle + (a \leftrightarrow b)\Big\}$$
$$= 16\nu\Big[|\nu| T^{\{a}_{ur}T^{b\}}_{vs} - T^{\{a}_{us}T^{b\}}_{vr}\Big] \,. \tag{B.21}$$

Inserting the last two into eqs. (B.13), (B.14), we see immediately that terms proportional to K cancel against each other.

Let us finally consider the spacetime dependence. After taking the spatial averages and time derivatives in eq. (2.30), omitting contact terms, and denoting $\tau_x = (x_0 - z_0)/T$, $\tau_y = (y_0 - z_0)/T$, we get

$$\partial_{x_0}\int_{\mathbf{x}} G(x-z) = h_1'(\tau_x) \,, \tag{B.22}$$
$$\partial_{x_0}\int_{\mathbf{x}} \partial_\mu G(x-z) = \frac{\delta_{\mu 0}}{T} \,, \tag{B.23}$$
$$\partial_{y_0}\int_{\mathbf{y}}\int_s \partial_\mu G(y-s)G(s-z) = -\delta_{\mu 0}T h_1(\tau_y) \,, \tag{B.24}$$
$$\partial_{y_0}\int_{\mathbf{y}}\int_s \partial_\mu\partial_\nu G(y-s)\partial_\nu G(s-z) = -\frac{\delta_{\mu 0}}{T} \,, \tag{B.25}$$
$$\partial_{x_0}\partial_{y_0}\int_{\mathbf{x},\mathbf{y}} G(x-y)\Big[\partial_\mu G(y-z)\Big]^2$$
$$= \frac{1}{V}\Big\{-f_1(\tau_y) + 2h_1'(\tau_x-\tau_y)\Big[h_1'(\tau_y) + 2\sum_{\mathbf{p}\neq\mathbf{0}}|\mathbf{p}|^2 C_{\mathbf{p}}(\tau_y)C_{\mathbf{p}}'(\tau_y)\Big]\Big\} \,, \tag{B.26}$$
$$\partial_{x_0}\partial_{y_0}\int_{\mathbf{x},\mathbf{y}} G(x-y)\partial_\mu G(x-z)\partial_\mu G(y-z)$$
$$= \frac{1}{V}\Big\{-h_1'(\tau_x)h_1'(\tau_y) + h_1'(\tau_x-\tau_y)\Big[h_1'(\tau_x) - h_1'(\tau_y)\Big] + h_1(\tau_x-\tau_y)\Big\} \tag{B.27}$$
$$= -\frac{1}{V}H(\tau_x,\tau_y) \,, \tag{B.28}$$
$$\partial_{x_0}\partial_{y_0}\int_{\mathbf{x},\mathbf{y}}\int_s\Big[G(x-s)G(y-s)\partial_\mu\partial_\nu G(s-z)\partial_\mu\partial_\nu G(s-z)$$
$$+\partial_\nu G(x-s)G(y-s)\partial_\mu G(s-z)\partial_\mu\partial_\nu G(s-z)$$
$$+G(x-s)\partial_\nu G(y-s)\partial_\mu G(s-z)\partial_\mu\partial_\nu G(s-z)$$
$$+\partial_\nu G(x-s)\partial_\nu G(y-s)\partial_\mu G(s-z)\partial_\mu G(s-z)\Big]$$
$$= 3\frac{G(0)}{T^2} + \frac{1}{2V}\Big\{h_1'(\tau_x)h_1'(\tau_y) + 7h_1'(\tau_x-\tau_y)\Big[h_1'(\tau_x) - h_1'(\tau_y)\Big]$$

$$
\begin{aligned}
&-3\Big[h_1(\tau_x-\tau_y)+h_1(\tau_x)+h_1(\tau_y)\Big]-4\Big[f_1(\tau_x)+f_1(\tau_y)\Big]\Big\} \\
&-\frac{4}{V}\sum_{\mathbf{p}\neq\mathbf{0}}\Big\{h_1'(\tau_x-\tau_y)|\mathbf{p}|^2\Big[C_{\mathbf{p}}(\tau_y)C_{\mathbf{p}}'(\tau_y)-C_{\mathbf{p}}(\tau_x)C_{\mathbf{p}}'(\tau_x)\Big]\Big\}\;. \qquad \text{(B.29)}
\end{aligned}
$$

The functions h_1, f_1, $C_{\mathbf{p}}$ appearing here have been defined in eqs. (2.26), (2.36), (2.37), respectively, and in eq. (B.28) we identified the function H defined in eq. (2.35). We also need to know that in dimensional regularization, $\partial_\mu^2 G(0)=1/V$ and

$$
G(0)=-\frac{\beta_1}{\sqrt{V}}\;, \qquad \text{(B.30)}
$$

where β_1 is a "shape coefficient" [28, 29]. It is furthermore useful to note the identity

$$
h_1'(\tau_x)h_1'(\tau_y)+h_1'(\tau_x-\tau_y)\Big[h_1'(\tau_x)-h_1'(\tau_y)\Big]=h_1(\tau_x-\tau_y)+h_1(\tau_x)+h_1(\tau_y)\;. \qquad \text{(B.31)}
$$

Summing all the results together, but making no assumptions about the form of $E(x)$, we obtain

$$
\begin{aligned}
&\lim_{m\to 0}(mV)^2T^2\partial_{x_0}\partial_{y_0}\int_{\mathbf{x}}\int_{\mathbf{y}}\Big\langle -\mathcal{P}^a(x)\mathcal{O}_{rsuv}(z)\mathcal{P}^b(y)\Big\rangle_\nu \\
&\quad=\Big[\nu^2T^{\{a}_{ur}T^{b\}}_{vs}-|\nu|T^{\{a}_{us}T^{b\}}_{vr}\Big]\times\Big\{1+\frac{2|\nu|T^2}{F^2V}\Big[h_1(\tau_x)+h_1(\tau_y)\Big] \\
&\qquad+\frac{2T}{F^2V}\Big[\partial_{x_0}\int_{\mathbf{x}}\int_s\partial_0G(z-s)E(s-x)+\partial_{y_0}\int_{\mathbf{y}}\int_s\partial_0G(z-s)E(s-y)\Big] \\
&\qquad+\frac{2T^2}{F^2}\partial_{x_0}\partial_{y_0}\int_{\mathbf{x},\mathbf{y}}E(x-y)\partial_\mu G(x-z)\partial_\mu G(y-z)\Big\} \\
&\quad+\Big[-|\nu|T^{\{a}_{ur}T^{b\}}_{vs}+\nu^2T^{\{a}_{us}T^{b\}}_{vr}\Big]\times\Big\{-\frac{2G(0)}{F^2} \\
&\qquad+\frac{T^2}{F^2V}\Big[f_1(\tau_x)+f_1(\tau_y)-h_1(\tau_x)-h_1(\tau_y)+H(\tau_x,\tau_y)\Big]\Big\}\;. \qquad \text{(B.32)}
\end{aligned}
$$

Taking finally the combinations in eq. (2.31); writing the result in the form of eq. (2.33); identifying expressions of the form in eq. (A.29) from the result; and inserting eq. (B.30) as well as the definition $\rho\equiv T/L$, we obtain

$$
\begin{aligned}
&\bar{\mathcal{A}}_\nu(x_0-z_0,y_0-z_0)\pm\tilde{\mathcal{A}}_\nu(x_0-z_0,y_0-z_0) \\
&\quad=\Big(1\mp\frac{1}{|\nu|}\Big)\Big\{\mathcal{B}_\nu(x_0-z_0)\mathcal{B}_\nu(y_0-z_0) \\
&\qquad+\frac{2\nu^2}{F^2}\partial_{x_0}\partial_{y_0}\int_{\mathbf{x},\mathbf{y}}E(x-y)\partial_\mu G(x-z)\partial_\mu G(y-z) \\
&\qquad\pm\frac{\nu^2}{F^2V}\Big[2\beta_1\rho^{-\frac{3}{2}}+f_1(\tau_x)+f_1(\tau_y)-h_1(\tau_x)-h_1(\tau_y)+H(\tau_x,\tau_y)\Big]\Big\}\;. \qquad \text{(B.33)}
\end{aligned}
$$

References

[1] M.K. Gaillard and B.W. Lee, Phys. Rev. Lett. 33 (1974) 108; G. Altarelli and L. Maiani, Phys. Lett. B 52 (1974) 351.

[2] N. Cabibbo, G. Martinelli and R. Petronzio, Nucl. Phys. B 244 (1984) 381; R.C. Brower, G. Maturana, M.B. Gavela and R. Gupta, Phys. Rev. Lett. 53 (1984) 1318.

[3] C.W. Bernard, T. Draper, A. Soni, H.D. Politzer and M.B. Wise, Phys. Rev. D 32 (1985) 2343.

[4] A. Jüttner, *Progress in kaon physics on the lattice,* [arXiv:0711.1239 [hep-lat]].

[5] J. Gasser and H. Leutwyler, Phys. Lett. B 188 (1987) 477; Nucl. Phys. B 307 (1988) 763.

[6] H. Neuberger, Phys. Rev. Lett. 60 (1988) 889; Nucl. Phys. B 300 (1988) 180.

[7] P.H. Ginsparg and K.G. Wilson, Phys. Rev. D 25 (1982) 2649.

[8] D.B. Kaplan, Phys. Lett. B 288 (1992) 342 [hep-lat/9206013].

[9] Y. Shamir, Nucl. Phys. B 406 (1993) 90 [hep-lat/9303005]; V. Furman and Y. Shamir, Nucl. Phys. B 439 (1995) 54 [hep-lat/9405004].

[10] R. Narayanan and H. Neuberger, Nucl. Phys. B 412 (1994) 574 [hep-lat/9307006]; Nucl. Phys. B 443 (1995) 305 [hep-th/9411108].

[11] H. Neuberger, Phys. Lett. B 417 (1998) 141 [hep-lat/9707022]; *ibid.* 427 (1998) 353 [hep-lat/9801031]; Phys. Rev. D 57 (1998) 5417 [hep-lat/9710089].

[12] P. Hasenfratz, Nucl. Phys. B 525 (1998) 401 [hep-lat/9802007].

[13] M. Lüscher, Phys. Lett. B 428 (1998) 342 [hep-lat/9802011].

[14] Y. Kikukawa and T. Noguchi, hep-lat/9902022.

[15] L. Giusti, C. Hoelbling, M. Lüscher and H. Wittig, Comput. Phys. Commun. 153 (2003) 31 [hep-lat/0212012].

[16] L. Giusti, P. Hernández, M. Laine, P. Weisz and H. Wittig, JHEP 11 (2004) 016 [hep-lat/0407007].

[17] L. Giusti, P. Hernández, M. Laine, C. Pena, J. Wennekers and H. Wittig, Phys. Rev. Lett. 98 (2007) 082003 [hep-ph/0607220].

[18] P. Hernández and M. Laine, JHEP 09 (2004) 018 [hep-ph/0407086].

[19] P. Hernández and M. Laine, JHEP 10 (2006) 069 [hep-lat/0607027].

[20] P. Hasenfratz, V. Laliena and F. Niedermayer, Phys. Lett. B 427 (1998) 125 [hep-lat/9801021].

[21] L. Giusti, P. Hernández, M. Laine, P. Weisz and H. Wittig, JHEP 01 (2004) 003 [hep-lat/0312012].

[22] S. Shcheredin and W. Bietenholz, PoS LAT2005 (2006) 134 [hep-lat/0508034] ;
W. Bietenholz and S. Shcheredin, Nucl. Phys. B 754 (2006) 17 [hep-lat/0605013].

[23] P. Dimopoulos *et al.*, Phys. Lett. B 641 (2006) 118 [hep-lat/0607028].

[24] L. Giusti, P. Hernández, M. Laine, P. Weisz and H. Wittig, JHEP 04 (2004) 013 [hep-lat/0402002].

[25] T.A. DeGrand and S. Schaefer, Comput. Phys. Commun. 159 (2004) 185 [hep-lat/0401011].

[26] P.H. Damgaard and K. Splittorff, Phys. Rev. D 62 (2000) 054509 [hep-lat/0003017].

[27] C.W. Bernard and M.F.L. Golterman, Phys. Rev. D 46 (1992) 853 [hep-lat/9204007]; S.R. Sharpe, Phys. Rev. D 46 (1992) 3146 [hep-lat/9205020].

[28] P. Hasenfratz and H. Leutwyler, Nucl. Phys. B 343 (1990) 241.

[29] F.C. Hansen, Nucl. Phys. B 345 (1990) 685; F.C. Hansen and H. Leutwyler, Nucl. Phys. B 350 (1991) 201.

[30] H. Leutwyler, Phys. Lett. B 189 (1987) 197.

[31] L. Del Debbio and C. Pica, JHEP 02 (2004) 003 [hep-lat/0309145]; L. Giusti, M. Lüscher, P. Weisz and H. Wittig, JHEP 11 (2003) 023 [hep-lat/0309189]; L. Del Debbio, L. Giusti and C. Pica, Phys. Rev. Lett. 94 (2005) 032003 [hep-th/0407052]; S. Dürr, Z. Fodor, C. Hoelbling and T. Kurth, JHEP 04 (2007) 055 [hep-lat/0612021].

[32] J. Wennekers and H. Wittig, JHEP 09 (2005) 059 [hep-lat/0507026].

[33] L. Giusti *et al*, in preparation.

[34] M. Lüscher, JHEP 12 (2007) 011 [arXiv:0710.5417 [hep-lat]].